Publication Year	2019
Acceptance in OA	2021-01-21T09:13:30Z
Title	Reclassification of Cepheids in the Gaia Data Release 2. Period-luminosity and period-Wesenheit relations in the Gaia passbands
Authors	RIPEPI, Vincenzo, MOLINARO, Roberto, MUSELLA, ILARIA, MARCONI, Marcella, LECCIA, Silvio, Eyer, L.
Publisher's version (DOI)	10.1051/0004-6361/201834506
Handle	http://hdl.handle.net/20.500.12386/29895
Journal	ASTRONOMY & ASTROPHYSICS
Volume	625

A&A 625, A14 (2019)
https://doi.org/10.1051/0004-6361/201834506
© ESO 2019

Astronomy & Astrophysics

Reclassification of Cepheids in the *Gaia* Data Release 2

Period-luminosity and period-Wesenheit relations in the *Gaia* passbands*

V. Ripepi[1], R. Molinaro[1], I. Musella[1], M. Marconi[1], S. Leccia[1], and L. Eyer[2]

[1] INAF-Osservatorio Astronomico di Capodimonte, Via Moiariello 16, 80131 Naples, Italy
e-mail: ripepi@oacn.inaf.it
[2] Department of Astronomy, University of Geneva, Ch. des Maillettes 51, 1290 Versoix, Switzerland

Received 24 October 2018 / Accepted 28 February 2019

ABSTRACT

Context. Classical Cepheids are the most important primary indicators for the extragalactic distance scale. Establishing the precise zero points of their period-luminosity and period-Wesenheit (PL/PW) relations has profound consequences on the estimate of H_0. Type II Cepheids are also important distance indicators and tracers of old stellar populations.
Aims. The recent Data Release 2 (DR2) of the *Gaia* spacecraft includes photometry and parallaxes for thousands of classical and Type II Cepheids. We seek to review the classification of *Gaia* DR2 Cepheids and to derive precise PL/PW for the Magellanic Clouds (MCs) and Galactic Cepheids.
Methods. We adopted information from the literature and the *Gaia* astrometry and photometry to assign DR2 Galactic Cepheids to the classical, anomalous, and Type II Cepheids classes.
Results. We reclassified the DR2 Galactic Cepheids and derived new precise PL/PW relations in the *Gaia* passbands for the MCs and Milky Way Cepheids. We investigated for the first time the dependence on metallicity of the PW relation for classical Cepheids in the *Gaia* bands, finding inconclusive results.
Conclusions. According to our analysis, the zero point of the *Gaia* DR2 parallaxes as estimated from classical and Type II Cepheids seems likely to be underestimated by ~0.07 mas, which agrees with recent literature. The next *Gaia* data releases are expected to fix this zero point offset to allow eventually a determination of H_0 to less than 1%.

Key words. stars: distances – stars: variables: Cepheids – distance scale

1. Introduction

Classical Cepheids (DCEPs) are the most important primary distance indicators for the cosmic distance scale (see e.g. Riess et al. 2016, 2018a) because of their characteristic period-luminosity (PL) and period-Wesenheit (PW) relations (Leavitt & Pickering 1912; Madore 1982; Caputo et al. 2000).

In conjunction with secondary distance indicators such as SNIa, the DCEPs provide an estimate of $H_0 \sim 73.48 \pm 1.66\,\mathrm{km\,s^{-1}\,Mpc^{-1}}$ with 2.3% of claimed uncertainty (Riess et al. 2018b). However, there is a tension at 3.4–3.7σ with $H_0 \sim 66.93 \pm 0.62\,\mathrm{km\,s^{-1}\,Mpc^{-1}}$ obtained from the analysis of the cosmic microwave background plus ΛCDM (Planck Collaboration Int. XLVI 2016; Riess et al. 2018a,b).

To reconcile the inconsistency between these values, we need more accurate calibrations of the different steps of the cosmic distance ladder. In first place we have to check the calibration of slopes/zero points of the PL/PW relations used for DCEPs, which currently rely on a handful of objects with accurate *Hubble* Space Telescope (HST) parallaxes (Riess et al. 2018a). In this context, measurements of the astrometric spacecraft *Gaia* (Gaia Collaboration 2016), which is collecting repeated multi-band photometric and astrometric data of sources over the entire sky to a limiting magnitude of about $G \sim 20.7$ mag, can help significantly. The *Gaia* Data Release 2 (DR2) (see Gaia Collaboration 2018, for a detailed description of the content of the release) has published photometry in the three *Gaia* passbands G, G_{BP}, and G_{RP}, as well as astrometry and radial velocity data obtained during the initial 22 months of data collection.

The multi-epoch *Gaia* data have permitted the study of an unprecedented number of variable stars of different types (for details see Holl et al. 2018). In particular, Clementini et al. (2019) discussed the pipeline of the *Cepheid&RRLyrae* Specific Object Studies (SOS) used to measure period(s), intensity-averaged G, G_{BP}, and G_{RP} magnitudes and amplitudes of pulsation for a sample of 140 784 RR Lyrae, and 9575 Cepheids. Among the latter, 3767, 3692, and 2116 are Cepheids belonging to the Large Magellanic Cloud (LMC), Small Magellanic Cloud (SMC), and all sky sample, respectively. The latter sample, consists essentially in candidate Cepheids belonging to our Galaxy. In the following we refer to these stars as the Milky Way (MW) sample. As a result of a complex concomitant factors, such as the automatic procedure and inaccurate parallaxes, the MW sample is thought to be significantly contaminated by non-cepheid types of variable stars (see Clementini et al. 2019, for details). Therefore, the main scope of this paper is to provide a detailed reclassification of the objects classified as Cepheids (of different types, see below) in Clementini et al. (2019), providing a comparison with the classification in the literature. We also aim at calculating empirical PL/PW relations in the *Gaia* passbands for the LMC/SMC and MW for future uses.

* Full Tables 2, 5, 7 and 8 are only available at the CDS via anonymous ftp to cdsarc.u-strasbg.fr (130.79.128.5) or via http://cdsarc.u-strasbg.fr/viz-bin/qcat?J/A+A/625/A14

Before proceeding, we distinguish three types of cepheid variables: DCEPs, anomalous Cepheids (ACEPs), and Type II Cepheids (T2CEPs). The latter type is usually subdivided into three subclasses, BL Her (BLHER), W Vir (WVIR), and RV Tau (RVTAU), in order of increasing periods. The DCEPs and ACEPs types are known to pulsate in different modes. In this paper we consider DCEPs pulsating in the fundamental, first overtone, second overtone[1], and multiple mode: we name these variables DCEP_F, DCEP_1O, DCEP_2O, DCEP_MULTI, respectively. Similarly, for ACEPs we distinguish objects pulsating in the fundamental (ACEP_F) and first overtone modes (ACEP_1O). For a detailed description of these classes of variability and their evolutionary status, see the recent textbook by Catelan & Smith (2015).

The manuscript is organised as follows: in Sect. 2 we derive empirical PL/PW relations for all type of Cepheids in the LMC/SMC; in Sect. 3 we present the results of the literature search and carry out the reclassification of the MW Cepheids; in Sect. 4 we calculate the PL/PW relations for the MW sample; and a brief summary closes the paper.

2. *Gaia* DR2 Cepheids in the magellanic clouds

Before facing the task of reclassifying the MW Cepheids in DR2, it is first useful to analyse the DR2 output for the MCs Cepheids.

In Clementini et al. (2016, 2019), i.e. for DR1 and DR2, respectively, we used PL/PW relations derived from OGLE-III[2] (Optical Gravitational Lensing Experiment) V, I photometry transformed in G, G_{RP} bands on the basis of Jordi et al. (2010) predicted colour transformations. It is then important to derive accurate PL/PW relations for the different types of Cepheids in the *Gaia* passbands directly from the actual data.

In DR2, 3767 and 3692 Cepheids of all types in the LMC and SMC were released, respectively (see Table 2 of Clementini et al. 2019, for full details). These samples were complemented with 61 and 73 Cepheids coming from the MW sample, but actually belonging to the LMC and SMC, respectively, as shown in Sect. 3.2.1 (see also Table 7). For DCEPs we first discarded multiple pulsators and used only objects with reliable values of the three G, G_{BP}, G_{RP} bands. We were then left with 1624 and 1207 DCEP_F and DCEP_1O pulsators in the LMC, as well as 1772 and 1368 DCEP_F and DCEP_1O pulsators in the SMC, respectively. We did not attempt to correct the classification of these objects because it had been already demonstrated that it is very accurate (see Fig. 41 in Clementini et al. 2019).

Secondly, we decided to use a different formulation of the Wesenheit magnitude with respect to that used in *Gaia* DR1 and DR2, involving only G and G_{RP} bands (see Clementini et al. 2016, 2019, for details). The new formulation is the following:

$$W(G, G_{BP}, G_{RP}) = G - \lambda(G_{BP} - G_{RP}), \quad (1)$$

where $\lambda = A(G)/E(G_{BP} - G_{RP})$. Empirically, it is known that the value of λ is of the order of 2 over a wide range of effective temperatures, including those typically spanned by Cepheids (Andrae et al. 2018). To obtain a more precise value, we adopted the synthetic photometry by Jordi et al. (2010), which provides the value of λ as a function of effective temperature, gravity, and metallicity. We selected the ranges of these parameters typical for Cepheids (i.e. $4500 < T_{\rm eff} < 7000$ K; $0.5 < \log g < 3.5$ dex; $-1 <$ [Fe/H] $< +0.5$ dex) and then averaged out the selected values, obtaining $\lambda = 1.95 \pm 0.05$, which is very close to the Andrae et al. (2018) result.

We tested this Wesenheit magnitude on DCEPs in the LMC, which are known to show very tight PW relations in all bands (see e.g. Soszyński et al. 2017a; Ripepi et al. 2012, in the optical and near-infrared, respectively). After a few experiments, we realised that the least-squares fit to the data gave a tighter PW relation (smaller scatter) if the λ value was slightly decreased to 1.90; the uncertainty was estimated of the order of 0.05, by looking at the value of λ that produced an increase in the dispersion. Hence, in the following we decided to use the ensuing Wesenheit magnitude:

$$W(G, G_{BP}, G_{RP}) = W = G - 1.90(G_{BP} - G_{RP}), \quad (2)$$

where G, G_{BP}, G_{RP} are the magnitudes in the *Gaia* bands. In comparison to that used in Clementini et al. (2016, 2019), the new formulation has the advantage to be linear in the colour term and to provide smaller dispersions in the PW relations.

Apart from the PW relation, we also derived individual PLs for the G, G_{BP}, G_{RP} bands. We did not attempt to correct for extinction because no reliable individual reddening estimate is present in the literature (see e.g. Gieren et al. 2018, for a discussion on the uncertainties in the individual reddening value for DCEPs). In any case, the average foreground reddening values in LMC and SMC are known to be small, of the order of $E(B-V) \approx 0.08$ and 0.04 mag, respectively (see e.g. the values from NASA/IPAC Extragalactic Database; NED[3]) so that extinction only affects the zero points of the PL relations, whereas the slope values are solid.

Operatively, to derive the relevant PL/PW relationships, we adopted a standard least-squares fitting procedure with σ clipping at 2.5–3σ level; typically 3 and 2.5 is used for PW and PL, respectively, because of the larger scatter in PL relations. The number of outliers is small because, as recalled above, the contamination of Cepheids in LMC and SMC is very small. It is important to note that for the DCEP_F in the SMC, we fitted two different lines in different period regimes characterised by values shorter or longer than ~2.95 days. This break in the PL/PW relations is well documented in the literature at all the wavelengths (see e.g. Subramanian & Subramaniam 2015; Ripepi et al. 2016, 2017). The result of the fitting procedure is shown in Table 1 and in Figs. 1 and 2. An inspection of Table 1 reveals that the PL and especially the PW relations for the LMC are less dispersed than those for the SMC. This is due to a depth effect generated by the well-known elongation of the SMC along the line of sight (see Ripepi et al. 2017, and references therein). We also note that the PW for the LMC is much less dispersed than the PLs both because the PW is not affected by reddening and because the colour term in the Wesenheit magnitude takes partially into account the intrinsic width of the instability strip. In the SMC there is less difference between the dispersion of PW and PLs because the dominant effect on the dispersion is the elongation along the line of sight.

As for the T2CEP variables, because of the paucity of the sample, we decided to use also objects without the G_{BP}, G_{RP} magnitudes to derive the PL relations in G. After some experiments, we decided to exclude RVTAU stars from the fits because they are too scattered and show a different slope of PL/PW with respect to BLHER and WVIR stars; this effect is well documented in the literature (see e.g. Soszyński et al. 2008; Matsunaga et al. 2009, 2011; Ripepi et al. 2015). The results of

[1] We note that second overtone pulsators were not classified by the *Cepheid&RRLyrae* SOS pipeline.

[2] http://ogle.astrouw.edu.pl/

[3] https://ned.ipac.caltech.edu/

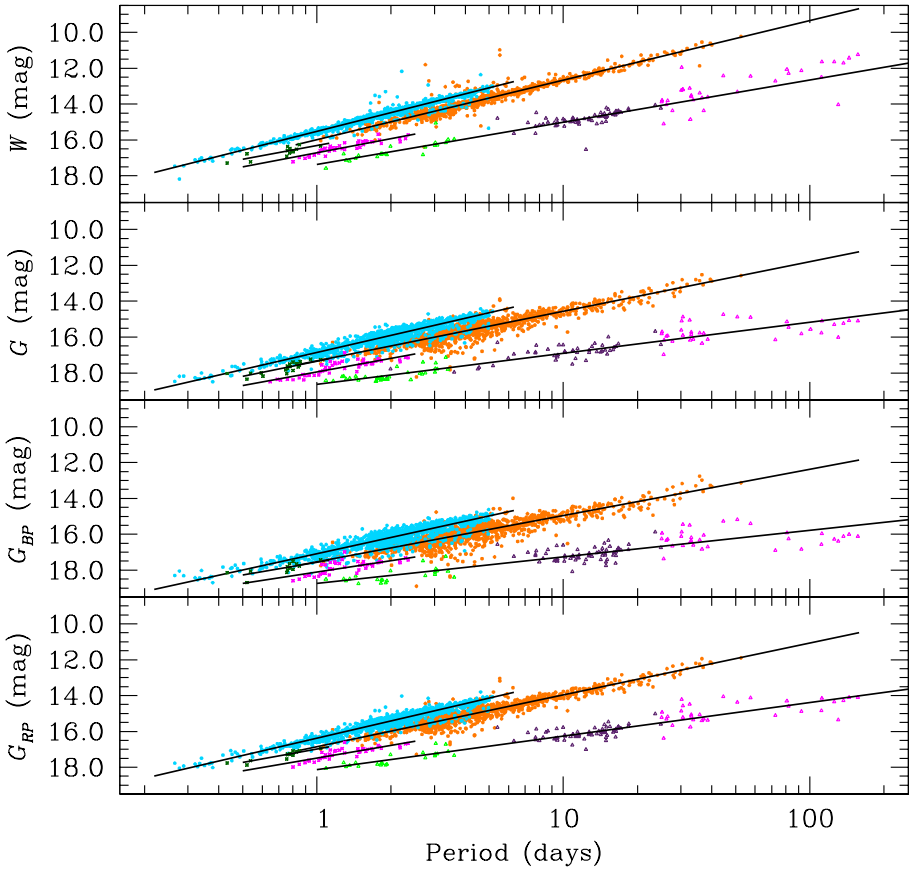

Fig. 1. For the LMC, PL/PW relations in the form $mag = \alpha + \beta \log P$. From *top* to *bottom panels*, *mag* is represented by the apparent W, G, G_{BP}, and G_{RP} magnitudes, respectively. Orange filled circles: DCEP_F; cyan filled circles: DECP_1O; magenta four-starred symbols: ACEP_F; dark green four-starred symbols: ACEP_1O; green open triangles: BLHER; violet open triangles: WVIR; and magenta open triangles: RVTAU.

the above procedure are listed in Table 1 and in Figs. 1 and 2. The T2CEP PL relations in the SMC for G_{BP}, G_{RP} bands were not calculated as the shortage of stars (only 15 usable objects) coupled with the large errors resulted in unreliable relationships.

We were also able to fit reasonable PL/PW relations for the ACEP_F and ACEP_1O variables in both the MCs. Also these results are presented in Table 1 and in Figs. 1 and 2. As a final remark, we underline that the PW and PL relations calculated in this paper (especially those in the G band) will be used in the SOS pipeline (Clementini et al. 2019) for the cepheid classification in the next *Gaia* Data Release 3.

3. Reclassification of *Gaia* MW DR2 Cepheids

3.1. Comparison with the literature

As anticipated in the introduction, the sample of MW Cepheids presented in the *Gaia* DR2 is most likely significantly contaminated and one of the purposes of this work is to clean it. To this aim, the first step consisted in a massive search for alternative classification in the literature. The largest databases of variable stars in the MW available are Simbad (Wenger et al. 2000) and VSX (The International Variable Star Index; Watson et al. 2006[4]). These sources have been complemented and completed by several additional literature works whose complete list is reported in the notes of Table 2. This table reports the source identification, equatorial coordinates, and variability classification given in *Gaia* DR2, as well as the literature name of the object, literature type(s) of variability, period(s) and source of this information. The acronyms for the variability types used in the table are listed in Table A.1. The analysis of periods in the literature is particularly important, as one cause of misclassification in DR2 is the wrong period found by the *Cepheids&RRLyrae* SOS pipeline, caused by the low number of epochs available for a consistent sample of objects; Clementini et al. (2019) analysed objects with more than 12 epochs.

Among the 2116 candidate Cepheids in the MW, 1416 have some mention in the literature. About 1008 of these have been classified in at least one of the cepheid subclasses, whereas 50 objects have a generic classification as "variables". The rest of the sample is composed by a disparate collection of variability types (see Tables 2 and A.1), even if a significant portion is represented by 121 variables classified as RR Lyrae. As expected, the cepheid sample in the MW from *Gaia* DR2 is actually contaminated by different variability types. The literature classification is also useful as a base for the specific reclassification, which is discussed in the next section.

3.2. Detailed reclassification

The procedure adopted for the reclassification relies on the visual inspection of each light curve (LC) and comparison with a reliable atlas of LCs such as that by the OGLE group[5] for the classical pulsating stars. The visual inspection of LCs was complemented by the analysis of the location of the stars in period-absolute Wesenheit magnitude, or astrometry-based luminosity, ABL, in case of negative parallaxes (see e.g. Arenou & Luri 1999, and Eq. (7) in the next section) and

[4] https://www.aavso.org/vsx/

[5] http://ogle.astrouw.edu.pl/atlas/index.html

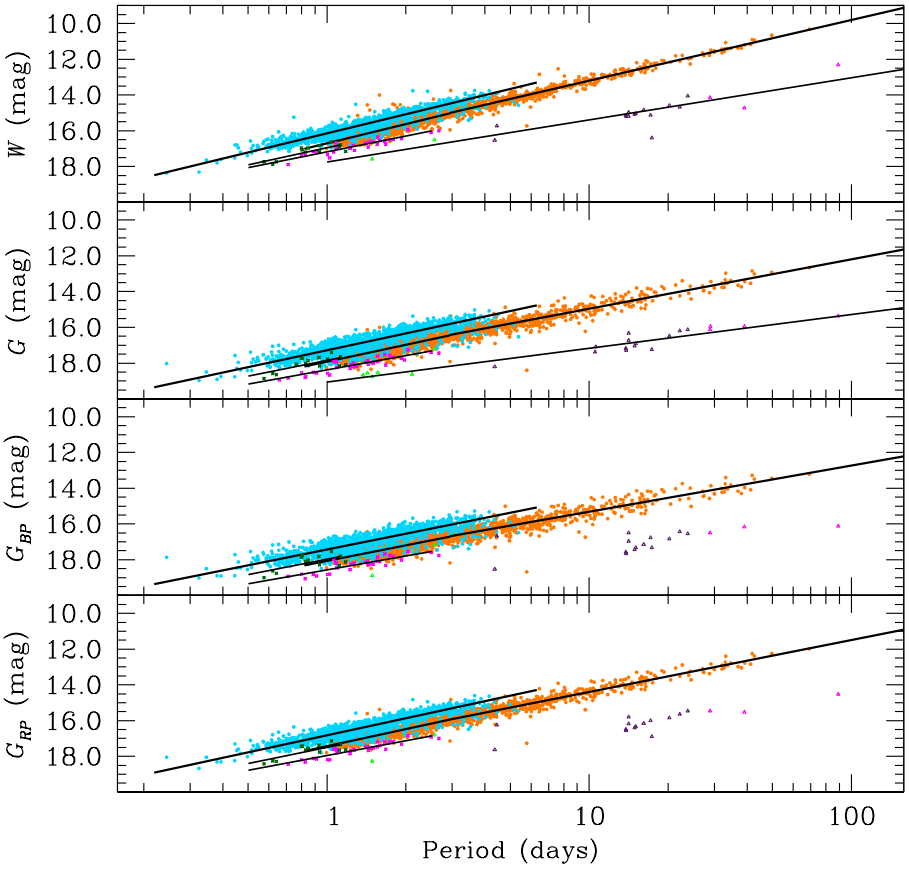

Fig. 2. As in Fig. 1 but for the SMC.

period-Fourier parameters (R_{21}, R_{31}, ϕ_{21}, ϕ_{31}) diagrams (for a definition of the Fourier parameters and their use in the *Gaia Cepheids&RRLyrae* SOS pipeline, see Clementini et al. 2016, 2019, and references therein). Additionally, we took into account the peak-to-peak amplitude ratio Amp(G_{BP})/Amp(G_{RP}) which, for the different types of Cepheids assumes characteristic values as shown in Table 4. The amplitude ratio is particularly useful to separate non-pulsating from pulsating variables, as the former type generally assumes values lower (∼1.0–1.2) than the latter (∼1.3–1.6).

We note that in building the PW/P−ABL diagrams we corrected the parallax zero point by adding 0.046 mas according to Riess et al. (2018b) (see also Schönrich & Eyer 2019, for a recent discussion on the zero point offset). This operation has little importance for the purpose of reclassifying the Cepheids, but is important for the determination of the absolute PW relations performed in the next section. The reclassification also made use of the literature classification, which was especially useful in the most doubtful cases. In particular, the use of periods from the literature helped to reclassify more than 140 objects whose LC shape clearly revealed the wrong period from *Gaia* DR2, which is generally caused by the low number of epochs available for these objects. In several of these cases, when sufficient data were available, we used the *Gaia* photometry to recalculate the periods using the literature values as a starting point and refining these values using *Period04* package (Lenz & Breger 2005). In this context, particularly useful was the work by Lemasle et al. (2018), who analysed in detail the multimode DCEPs in DR2, providing a list of reliable new multimode candidates.

As for the types of variability, our reclassification is restricted to all subtypes of cepheid variables that are the main target of the present work. Apart from these objects, we only classified in detail RR Lyrae and ACEP stars. We classified the former because their characteristic LCs make these sources relatively easy to identify and because they are analysed together with Cepheids in the *Gaia Cepheids&RRLyrae* SOS pipeline. As for the ACEPs, they were absent in the *Cepheids&RRLyrae* SOS pipeline (see Clementini et al. 2019), but several literature works reported their presence in the MW (e.g. OGLE group). Moreover during the process of reclassification, we realised that the LC shape for some short (1–2 days) period Cepheids did not fit completely neither with DCEPs nor with BLHERs. Therefore, we adopted the usual classification scheme for ACEPs in terms of ACEP_F and ACEP_1O. We note that in the absence of very precise distances (the candidate ACEPs are in general faint), the distinction between ACEP_1O and DCEP_1O on the basis of the LC shapes is very difficult because at fixed period the LCs of these two classes are very similar. Similarly, ACEP_Fs with periods shorter or longer than one day can be confused with RRABs or DCEP_Fs, respectively. The distinction between ACEPs and DCEPs is favoured by the position of the object in the MW; high Galactic latitude DCEPs are unlikely. However RRABs are ubiquitous in the Galaxy and a similar separation cannot be carried out. The distinction between these classes will be greatly facilitated by the availability of more precise parallaxes, as expected from the next *Gaia* data releases. Finally, the classification types considered in this work are as follows: DCEP_F, DCEP_1O, DCEP_2O, DCEP_MULTI[6], ACEP_F, ACEP_1O,

[6] DCEP_MULTI class is in turn subdivided into subclasses according to the period ratios of the modes pulsating simultaneously, for example fundamental/first overtone (F/1O). In this paper when we classify an object as DCEP_MULTI, we are assuming that the period ratios found in the *Gaia* DR2 are correct.

Table 1. Results of the least-squares fit in the form $mag = \alpha + \beta \log P$ for the LMC and SMC, where *mag* is represented by the Wesenheit magnitudes W (calculated as in Eq. 2) or by the G, G_{BP}, G_{RP} magnitudes.

Galaxy (1)	α (2)	β (3)	σ (4)	n (5)	Method (6)	Type (7)	Note (8)
LMC	16.000±0.008	−3.327 ± 0.012	0.104	1539	PW	DCEP_F	
LMC	15.518±0.004	−3.471 ± 0.012	0.087	1148	PW	DCEP_1O	
LMC	17.326±0.014	−2.765 ± 0.021	0.191	1545	PL(G)	DCEP_F	
LMC	16.860±0.010	−3.159 ± 0.029	0.209	1158	PL(G)	DCEP_1O	
LMC	17.545±0.017	−2.580 ± 0.025	0.229	1545	PL(G_{BP})	DCEP_F	
LMC	17.088±0.012	−3.008 ± 0.035	0.258	1176	PL(G_{BP})	DCEP_1O	
LMC	16.859±0.012	−2.892 ± 0.018	0.159	1542	PL(G_{RP})	DCEP_F	
LMC	16.384±0.008	−3.204 ± 0.023	0.169	1157	PL(G_{RP})	DCEP_1O	
SMC	16.705±0.015	−3.595 ± 0.057	0.209	1126	PW	DCEP_F	$P < 2.95$ d
SMC	16.608±0.021	−3.400 ± 0.026	0.169	608	PW	DCEP_F	$P \geq 2.95$ d
SMC	17.294±0.027	−2.897 ± 0.034	0.219	613	PW	DCEP_1O	
SMC	16.823±0.008	−3.160 ± 0.031	0.221	1259	PL(G)	DCEP_F	$P < 2.95$ d
SMC	16.137±0.006	−3.555 ± 0.025	0.175	1226	PL(G)	DCEP_F	$P \geq 2.95$ d
SMC	17.916±0.017	−3.113 ± 0.063	0.231	1110	PL(G)	DCEP_1O	
SMC	17.722±0.030	−2.764 ± 0.037	0.238	598	PL(G_{BP})	DCEP_F	$P < 2.95$ d
SMC	17.274±0.009	−3.134 ± 0.037	0.262	1264	PL(G_{BP})	DCEP_F	$P \geq 2.95$ d
SMC	18.066±0.016	−2.892 ± 0.063	0.229	1102	PL(G_{BP})	DCEP_1O	
SMC	17.891±0.035	−2.578 ± 0.043	0.275	607	PL(G_{RP})	DCEP_F	$P < 2.95$ d
SMC	17.431±0.010	−2.944 ± 0.040	0.286	1287	PL(G_{RP})	DCEP_F	$P \geq 2.95$ d
SMC	17.425±0.014	−3.153 ± 0.054	0.201	1132	PL(G_{RP})	DCEP_1O	
LMC	16.725±0.033	−2.625 ± 0.196	0.143	38	PW	ACEP F	
LMC	16.314±0.087	−2.564 ± 0.506	0.166	13	PW	ACEP 1O	
LMC	17.948±0.034	−2.516 ± 0.201	0.189	46	PL(G)	ACEP F	
LMC	17.355±0.074	−2.749 ± 0.455	0.173	19	PL(G)	ACEP 1O	
LMC	18.115±0.052	−2.119 ± 0.304	0.225	38	PL(G_{BP})	ACEP F	
LMC	17.561±0.111	−2.401 ± 0.649	0.212	13	PL(G_{BP})	ACEP 1O	
LMC	17.496±0.036	−2.354 ± 0.209	0.154	38	PL(G_{RP})	ACEP F	
LMC	16.992±0.056	−2.486 ± 0.327	0.107	13	PL(G_{RP})	ACEP 1O	
SMC	17.185±0.042	−2.931 ± 0.229	0.170	31	PW	ACEP F	
SMC	16.942±0.078	−3.211 ± 0.659	0.213	13	PW	ACEP 1O	
SMC	18.380±0.041	−2.669 ± 0.223	0.188	36	PL(G)	ACEP F	
SMC	17.836±0.096	−2.943 ± 0.843	0.284	15	PL(G)	ACEP 1O	
SMC	18.569±0.052	−2.598 ± 0.280	0.207	31	PL(G_{BP})	ACEP F	
SMC	17.966±0.111	−2.883 ± 0.944	0.305	13	PL(G_{BP})	ACEP 1O	
SMC	17.954±0.039	−2.754 ± 0.209	0.155	31	PL(G_{RP})	ACEP F	
SMC	17.489±0.088	−3.017 ± 0.750	0.243	13	PL(G_{RP})	ACEP 1O	
LMC	17.376±0.049	−2.356 ± 0.050	0.162	80	PW	T2CEP	
LMC	18.627±0.055	−1.726 ± 0.061	0.251	112	PL(G)	T2CEP	
LMC	18.743±0.088	−1.484 ± 0.093	0.303	82	PL(G_{BP})	T2CEP	
LMC	18.132±0.069	−1.875 ± 0.072	0.238	83	PL(G_{RP})	T2CEP	
SMC	17.755±0.197	−2.359 ± 0.183	0.233	15	PW	T2CEP	
SMC	19.063±0.147	−1.893 ± 0.145	0.271	20	PL(G)	T2CEP	

Notes. The different columns show the: (1) studied galaxy; (2) and (3) coefficients of the linear regression and relative errors; (4) rms of the residuals; (5) number of objects used in the fit; (6) method (PL or PW); (7) type of pulsator; and (8) notes.

BLHER, WVIR, RVTAU, CEP, RRAB, RRC, OTHER, where CEP means that the object is a cepheid candidate but we could not determine the type.

Before proceeding with the analysis (i.e. the construction of PW/P−ABL diagrams), we checked the goodness of the *Gaia* astrometric solution for the 2116 MW DR2 Cepheids. According to Lindegren et al. (2018) a parameter measuring the goodness of the fit is the *astrometric_excess_noise* (ϵ_i), measuring the excess of noise of the source. If $\epsilon_i > 0$, the residuals are statistically larger than expected. The additional parameter *astrometric_excess_noise_sig* (D) measures the significance of ϵ_i. If $D \leq 2$ then ϵ_i is probably not significant and the source could have a good astrometric solution even if ϵ_i is large. More recently, Lindegren (2018) devised a new parameter called the renormalised unit weight error (RUWE) that is not part of the official *Gaia* DR2; this parameter consists in a renormalisation

Table 2. Table with the literature classification for 1416 objects among the 2116 candidate Cepheids in the MW by Clementini et al. (2019).

Source_id	RA	Dec	DR2 Class.	Lit. Name	Lit. Class.
	deg	deg			
(1)	(2)	(3)	(4)	(5)	(6)
2947530506428832768	101.64608	−14.92456	DCEP_1O	ASAS J064635-1455.5	DSCT/SXPHE
208360790657462144	79.45432	44.47322	WVIR	ASASSN-V J051749.04+442823.6	RRAB
3315820030750497536	89.13874	1.70906	DCEP_1O	CRTS J055633.2+014232	RRd
4044404165342126848	276.27275	−34.44904	DCEP_MULTI	V3276 Sgr	RRAB
4071594911751759872	280.72338	−28.62898	DCEP_1O	[CAG2000] vs1f408	RRC
3045809872243862400	106.25278	−11.81071	DCEP_1O	GDS_J0705006-114838	VAR
4122020821451345664	259.72364	−19.99288	DCEP_1O	V1836 Oph	RR
4051686608879712640	277.11621	−27.4369	DCEP_1O	MACHO 175.30920.52	RRAB
3099348185775497728	101.98331	−7.41384	BLHER	ASASSN-V J064755.99-072449.9	RRAB
4114405122877842688	257.82295	−23.27459	DCEP_MULTI	140805	RRAB
4077490291331290368	278.75571	−24.01232	DCEP_1O	124321	RRC
4043821561616680448	270.95217	−31.78211	RVTAU	OGLE-BLG-RRLYR-12209	RRAB
4627678075752483584	65.96439	−76.91188	BLHER	OGLE-GAL-ACEP-006	ACEP/DCEP_F
4072780464535420160	279.21002	−26.99927	DCEP_F	[CAG2000] vs11f595	RRAB
4594729766718946304	265.52038	27.75574	DCEP_1O	28630	RRAB

Continuation

Lit. source	P1	P2	P3	P1 source	P2 source	P3 source
	days	days	days			
(7)	(8)	(9)	(10)	(11)	(12)	(13)
VSX/ASAS_RICHARDS	0.0954	–	–	VSX/ASAS_RICHARDS	–	–
ASAS-SN	0.1849	–	–	ASAS-SN	–	–
CRTS	0.2731	–	–	CRTS	–	–
VSX	0.3565	–	–	VSX	–	–
VSX	0.3920	–	–	VSX	–	–
VSX/PS1	0.4276	–	–	PS1	–	–
VSX	0.4342	–	–	VSX	–	–
VSX	0.4675	–	–	VSX	–	–
ASAS-SN	0.4820	–	–	ASAS-SN	–	–
PS1	0.4838	–	–	PS1	–	–
PS1	0.4895	–	–	PS1	–	–
OGLE	0.4959	–	–	OGLE	–	–
OGLE/VSX	0.5042	1.8836	–	OGLE	VSX	–
VSX	0.5048	–	–	VSX	–	–
PS1	0.5049	–	–	PS1	–	–

Notes. The different columns correspond to the following: (1) *Gaia* DR2 source identification; (2)-(3) RA-Dec (J2000); (4) variability classification according to *Gaia* DR2; (5) name of the object in the literature; (6) type(s) of variability found in the literature; (7) source for the different type of variability, separated by a "/" or "//" depending whether or not the period estimates of the two or more sources agree; (8)-(10) period(s) present in the literature; (11)-(13) sources of the period(s) in columns (8)-(10). A glossary of the variability types is reported Table A.1. The acronyms for the literature are given in the references of this table. The table is published in its entirety at the CDS. A portion including the first 15 lines is shown for guidance regarding its form and content.

References. ASAS3 (All Sky Automated Survey, Pojmanski 1997, 2002); ASAS_RICHARDS (All Sky Automated Survey re-classification, Richards et al. 2012); ASAS-SN (All-Sky Automated Survey for Supernovae, Jayasinghe et al. 2018); B15 (Berdnikov et al. 2015); C01 (Clement et al. 2001); CRTS (Catalina Real-Time Transient Survey, Drake et al. 2014, 2017); GCVS (General Catalogue of Variable Stars, Samus' et al. 2017); DR1 (Clementini et al. 2016); EROS2_KIM (Kim et al. 2014); Hip11 (Dubath et al. 2011); IOMC (Integral Optical Monitoring Camera, Alfonso-Garzón et al. 2012); Kep11 (Debosscher et al. 2011); LINEAR (Lincoln Near-Earth Asteroid Research, Palaversa et al. 2013); NSVS (Northern Sky Variable Survey, Woźniak et al. 2004; Hoffman et al. 2009); OGLE (Optical Gravitational Lensing Experiment, Soszyński et al. 2015a,b, 2016, 2017a,b, 2018); PS1 (Panoramic Survey Telescope & Rapid Response System, Sesar et al. 2017); SDSS (Ivezić et al. 2007); Simbad (Wenger et al. 2000); VSX (The International Variable Star Index, Watson et al. 2006).

of the astrometric χ^2. According to Lindegren (2018) values of RUWE $\leq$ 1.4 should indicate good astrometry. We cross-matched the two indicators and decided to take as objects with good astrometry those with RUWE $\leq$ 1.4, $\epsilon_i \leq 1$, $D \leq 2$, resulting in 151 out of 2116 stars with astrometry that is not reliable. The position of these stars in the PW/P−ABL relations was not taken into account for the classification, which then was based only on the shape of the LCs and on Fourier parameters.

Having set out all the tools, we proceeded with the reclassification by looking first at the position of the star in the PW/P−ABL relations. Because of the large relative error on parallax, the position of the targets in these diagrams is often ambiguous, i.e. compatible with different cepheid types. This

Table 3. Results of the least-squares fit in the form of Eq. (7) or Eq. (11) for the full MW DCEPs and T2CEPs sample (top part of the table) and for the selected sample of MW DCEPs with a full characterisation in terms of reddening and metallicity estimates (bottom half part of the table).

α (1)	β (2)	γ (3)	$\sigma_{\rm ABL}$ (4)	n (5)	Method (6)	Type (7)
Full MW DCEPs and T2CEPs sample						
-2.701 ± 0.086	-3.320 ± 0.107		0.013	489	PW_A	DCEP_F
-2.976 ± 0.131	-4.095 ± 0.304		0.020	138	PW_A	DCEP_1O
-1.194 ± 0.061	-2.381 ± 0.080		0.071	269	PW_A	T2CEP
-2.699 ± 0.023	-3.327 fixed		0.013	489	PW_A	DCEP_F
-3.246 ± 0.045	-3.471 fixed		0.020	138	PW_A	DCEP_1O
-1.211 ± 0.043	-2.356 fixed		0.071	269	PW_A	T2CEP
Selected MW DCEPs sample						
-2.837 ± 0.081	-3.183 ± 0.097		0.011	292	PW_A	DCEP_F
-3.214 ± 0.223	-3.587 ± 0.507		0.012	33	PW_A	DCEP_1O
-1.942 ± 0.096	-2.454 ± 0.116		0.025	273	$PL(G^0_A)$	DCEP_F
-1.903 ± 0.302	-3.709 ± 0.712		0.026	33	$PL(G^0_A)$	DCEP_1O
-1.816 ± 0.102	-2.229 ± 0.121		0.031	273	$PL(G^0_{BP,A})$	DCEP_F
-2.100 ± 0.178	-2.776 ± 0.375		0.022	33	$PL(G^0_{BP,A})$	DCEP_1O
-2.313 ± 0.094	-2.607 ± 0.113		0.019	273	$PL(G^0_{RP,A})$	DCEP_F
-2.637 ± 0.178	-3.110 ± 0.383		0.016	33	$PL(G^0_{RP,A})$	DCEP_1O
-2.721 ± 0.025	-3.327 fixed		0.011	292	PW_A	DCEP_F
-3.261 ± 0.056	-3.471 fixed		0.012	33	PW_A	DCEP_1O
-1.688 ± 0.032	-2.765 fixed		0.025	273	$PL(G^0_A)$	DCEP_F
-2.175 ± 0.072	-3.159 fixed		0.028	33	$PL(G^0_A)$	DCEP_1O
-1.525 ± 0.033	-2.580 fixed		0.031	273	$PL(G^0_{BP,A})$	DCEP_F
-1.855 ± 0.040	-3.308 fixed		0.023	33	$PL(G^0_{BP,A})$	DCEP_1O
-2.083 ± 0.030	-2.892 fixed		0.019	273	$PL(G^0_{RP,A})$	DCEP_F
-2.593 ± 0.042	-3.204 fixed		0.016	33	$PL(G^0_{RP,A})$	DCEP_1O
-2.862 ± 0.082	-3.134 ± 0.095	-0.237 ± 0.199	0.011	261	PW_AZ	DCEP_F
-2.716 ± 0.028	-3.327 fixed	-0.105 ± 0.207	0.011	261	PW_AZ	DCEP_F

Notes. The different columns show the: (1–3) coefficients of the nonlinear fit and the relative errors; (4) rms of the residuals of the ABL function; (5) number of objects used in the fit; (6) method (PL or PW); (7) type of the pulsators. To remark on the differences with Table 1, we added an underscript "A" or a superscript 0 to show that the magnitudes adopted are absolute and/or de-reddened, respectively. "Fixed" means that the slope of LMC (β) was imposed to derive the other parameters; PW_AZ indicates a PW relation depending on metallicity.

occurs in particular for periods shorter than three days, i.e. characteristics of DCEPs, ACEPs and BLHERs. Moreover, DCEPs and WVIRs candidate positions largely overlap when the relative error on the parallax is larger than ∼30%. We then passed to a visual inspection of the LCs and of the period-Fourier parameters diagrams. Particularly useful were the P-R_{21} and the P-ϕ_{21} diagrams to separate DCEP_F from DCEP_1O and low-period DCEP_F from ACEP_F and BLHER, respectively. Despite all these efforts, in some cases the classification of Cepheids with sawtooth LC shape and periods ∼1−2 days was difficult, as the shape of the LCs of DCEP_F, ACEP_F, and BLHER are very similar in this period range and the differences can only be revealed in very well sampled and precise LCs; this condition is not always fulfilled in our case. Also the position of these objects in the P-ϕ_{21} diagram was sometimes not conclusive. In some ambiguous cases we assigned to the ACEP class objects with high Galactic latitude, as we do not expect DCEPs in the MW halo. A similar distinction cannot be carried out between BLHER and ACEPs, as these classes share the same locations in the MW. In any case, the classification of these objects might be subject to a revision when more accurate *Gaia* parallaxes and metallicity estimates are available, given that both ACEPs and BLHERs are expected to be more metal poor with respect to DCEPs; this classification will allow us to disentangle clearly the PL/PW relations for the different cepheid types as occurs in the LMC/SMC. For 13 objects with clear cepheid-like LC and

Table 4. Average peak-to-peak amplitude ratio Amp(G_{BP})/Amp(G_{RP}) for the different types of Cepheids considered in this work.

Type	Amp. ratio	Dispersion
DCEP_F	1.58	0.10
DCEP_1O	1.63	0.07
ACEP	1.54	0.20
BLHER	1.53	0.14
WVIR	1.33	0.14
RVTAU	1.45	0.25

Notes. We note that the values listed in the table were calculated on the reclassified sample.

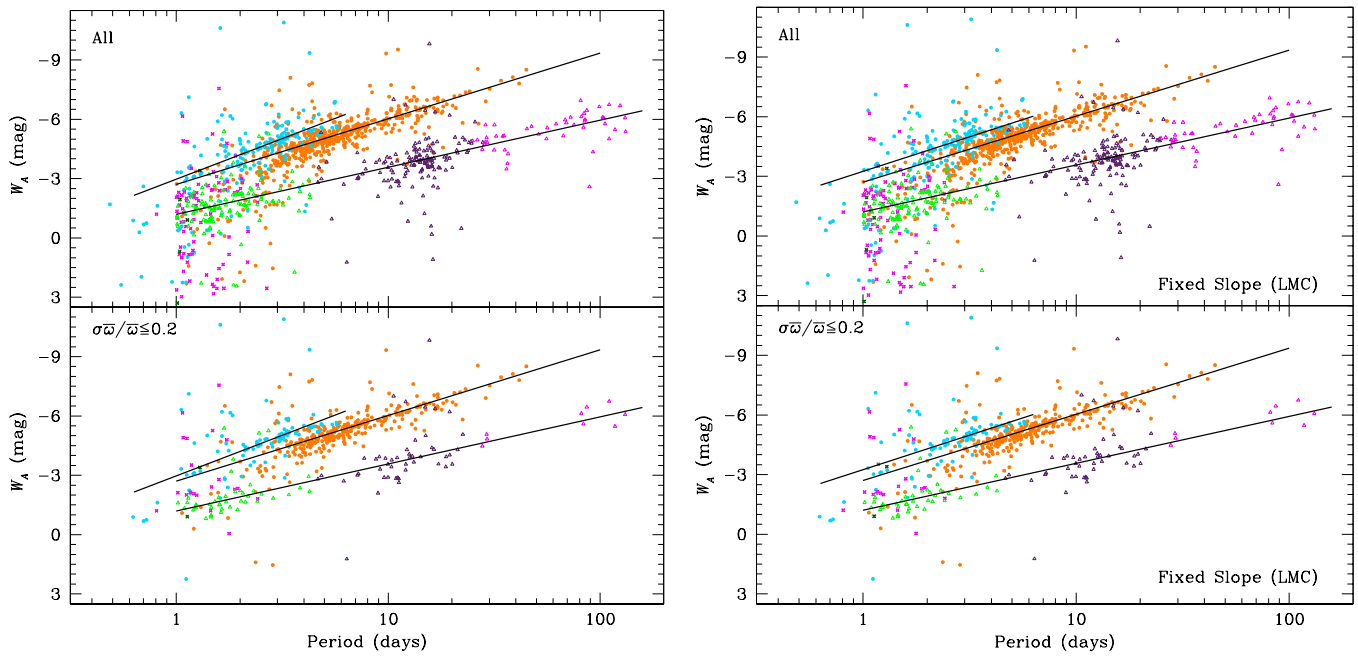

Fig. 3. Results for the reclassified MW sample: PW relations. The colour code is as in Fig. 1. *Top* and *bottom panels*: complete sample and that with relative error on parallax better than 20%, respectively. The solid lines represent the least-squares fit to the data obtained with the ABL method (see text). The PW relations are of the form $W_A = \alpha + \beta \log P$. *Left panels*: PW relations obtained with β coefficient treated as unknown parameter in Eq. (7). *Right panels*: β coefficient fixed and equal to that obtained from the LMC.

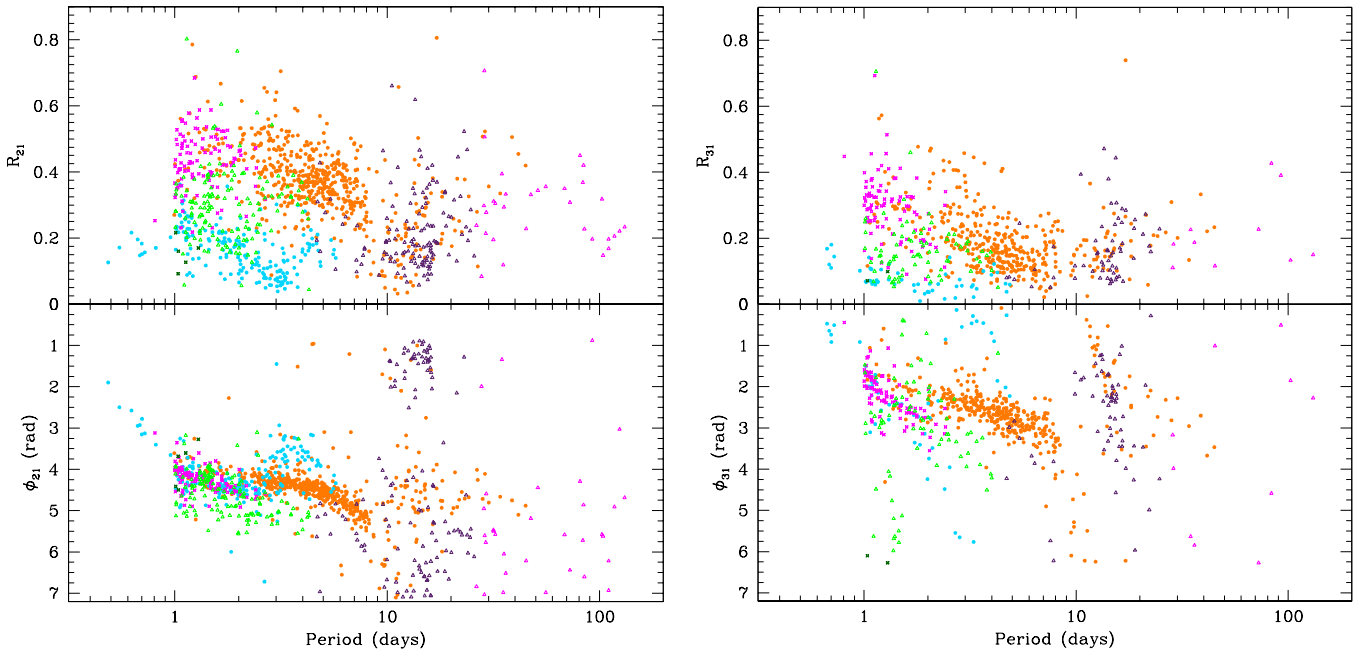

Fig. 4. Fourier parameters for the reclassified objects. The colour code is as in Fig. 1.

correct position in the P-Fourier parameters diagrams we were not able to assign a more precise type, and we indicated these sources with CEP. Their detailed subclassification will be determined using future *Gaia* releases.

The result of the procedure described above is shown in Table 5, in which we report for each of the 2116 MW Cepheids the new classification and all the data from *Gaia* DR2 used in the reclassification process. These include the parameters to estimate the goodness of the astrometry and the parameter E(BP/RP), indicating the excess of flux in the G_{BP}, G_{RP} bands with respect to the G band. Values larger than 2 usually indicate problems with colours. This parameter is reported for completeness but it affects very few objects. A detailed description of the different columns can be found in the table caption. In the notes (last column) we report special cases, for example when the literature period was used or the astrometry was not usable. An inspection of the table reveals that no classification was possible for 128 objects for various reasons specified in the notes, of which the most common are the lack of precise parallaxes or LCs that are scanty or incomplete. A total of 1257 stars

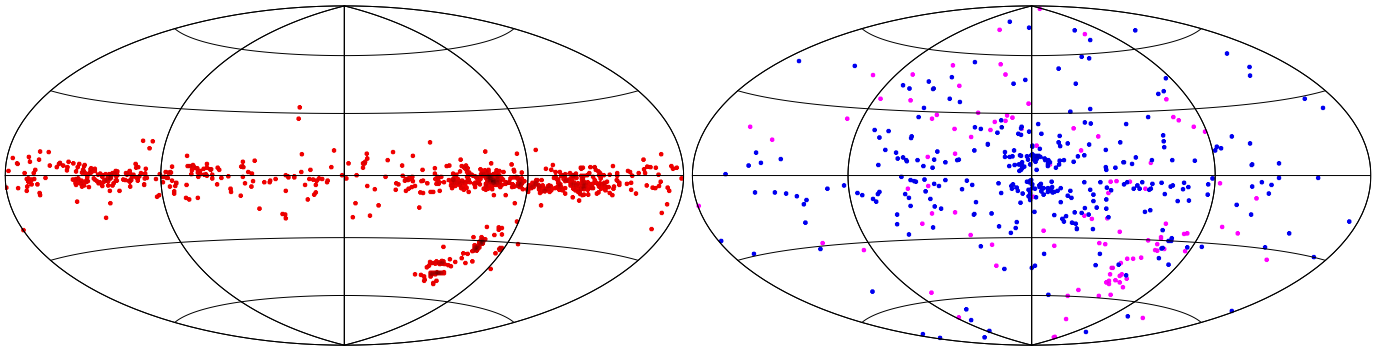

Fig. 5. Aitoff projection in Galactic coordinates of the objects reclassified in this work. *Left panel*: DCEPs (pulsating in any mode: red filled circles). *Right panel*: T2CEPs (of any type: blue filled circles) and ACEPs (pulsating in any mode: magenta filled circles).

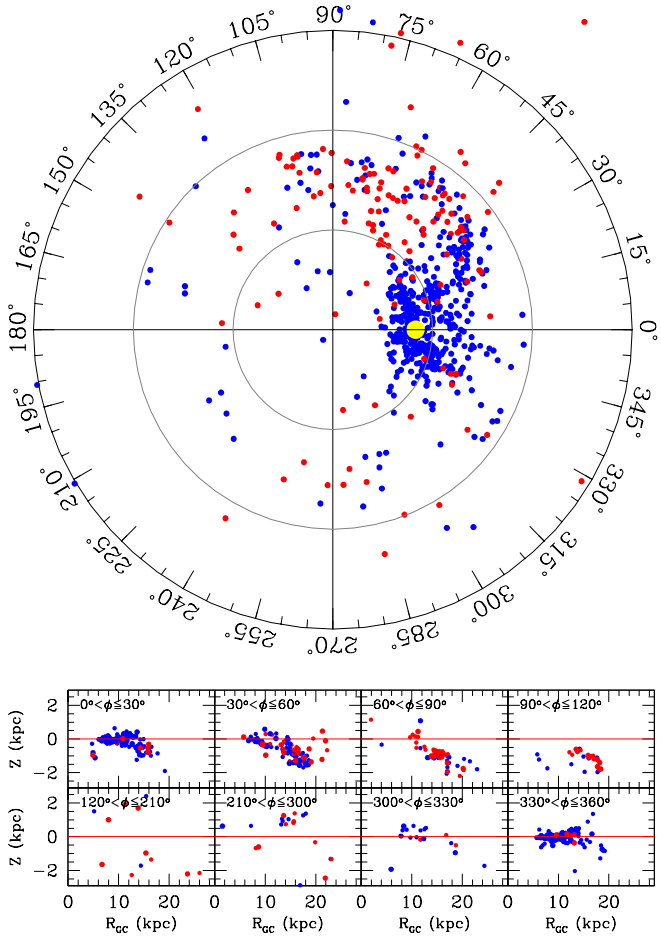

Fig. 6. *Top panel*: polar map of the Galactic plane depicted by known (blue filled circles) and newly discovered (red filled circles) DCEPs (pulsating in any mode). The Galactic centre is in the middle; the circles have radii of 10, 20, and 30 kpc, respectively. A yellow disc represents the position of the Sun. We note that the Galactocentric polar coordinate Φ is 0° in the direction of the Sun. *Bottom panel*: distribution of the distances from the Galactic plane (Z) as a function of the Galactocentric distance (R_{GC}) for different intervals of Φ. The warping of the disc is clearly visible.

have been classified as Cepheids of any type: 84 objects as RR Lyrae and 647 as variables of other type (in addition to the 128 stars with no classification).

An overall comparison of the new classification for the 1257 Cepheids with the literature is shown in Table 6. An inspection of the table shows that we changed the literature classification for 270 objects, whereas 274 are new Cepheids completely unknown in the literature or indicated as variable.

To visualise the results, we show in Fig. 3 (top panels) the PW relations for the stars classified as Cepheids except those with negative parallaxes (203 objects). Error bars are not shown for clarity reasons. The different types of variables are identified in the figure with different colours (see caption of the figure). An inspection of the figure reveals that because of the large errors in parallaxes, objects belonging to different cepheid types are mixed and it is not easy to define tight PW relations as those for the LMC/SMC. The situation is improved if we restrict to objects with relative error on parallaxes lower than 20%. This is shown in the bottom panels of Fig. 3.

We can compare these results with those reported in Fig. 7 of Clementini et al. (2019). A large part of the objects below the dashed line in that figure, more than 700 objects that were expected to be contaminating stars, now disappear and are classified as "OTHER" or not classified; about 150 of these were known in the literature as non-pulsating variables (see Table 2). However not all the objects in the lower part of the diagram disappeared, as several objects that are clearly cepheid variables can be found several magnitudes below (some also above) the relevant PW sequence. This is not surprising since, among the other issues: First, the astrometric solution for DR2 did not take into account duplicity and therefore the presence of companions can not only affect the photometry, but also the parallax. Second, the chromatic correction for the astrometric solution is based on the mean magnitude and not on the epoch colour (see Lindegren et al. 2018).

The P-R_{21}/ϕ_{21} and P-R_{31}/ϕ_{31} diagrams for the reclassified Cepheids are shown in Fig. 4. A comparison with the similar Figs. 37 and 38 of Clementini et al. (2019) shows that the sequences of the different types of Cepheids are now better defined and more congruent with those in the MCs.

Similarly, the location on the sky in Galactic coordinates for the reclassified Cepheids is shown in Fig. 5. Left and right panels of the figure display the location of DCEPs and ACEPs/T2CEPs, respectively. The DCEPs are now located preferentially along the MW disc, as expected for this population I stars, whereas ACEP/DCEP are distributed more homogeneously across the MW including the centre and the halo, as expected (compare with Fig. 39 in Clementini et al. 2019).

3.2.1. Cepheid stars hosted by stellar clusters or dwarf galaxies orbiting the MW

Having completed the reclassification, we checked whether some of the objects comprised in the MW sample are actually

Table 5. Table with the new classification.

Source_id	RA	Dec	n_G	$n_{G_{BP}}$	$n_{G_{RP}}$	Period	G	G_{BP}	G_{RP}	R_{21}	R_{31}
	deg	deg				days	mag	mag	mag		
(1)	(2)	(3)	(4)	(5)	(6)	(7)	(8)	(9)	(10)	(11)	(12)
2947530506428832768	101.64608	−14.92456	19	17	17	0.09537	12.677	12.997	12.22	99.999	99.999
3315820030750497536	89.13874	1.70906	14	14	14	0.27332	16.263	17.001	15.385	0.086	0.131
4071594911751759872	280.72338	−28.62898	14	14	14	0.39195	16.182	16.4	15.775	0.186	99.999
4122020821451345664	259.72364	−19.99288	20	16	16	0.43408	16.396	16.761	15.785	0.287	99.999
4296338318281270144	293.05243	8.93232	32	28	32	0.44584	16.755	17.361	15.992	0.136	0.133
6641655551574932992	298.6506	−53.31556	32	31	31	0.45379	13.83	14.016	13.499	0.13	99.999
5631368811358200320	141.58416	−31.61573	19	16	17	0.46519	16.371	16.604	15.981	0.229	99.999
4051686608879712640	277.11621	−27.4369	17	16	16	0.46752	15.764	16.085	15.262	99.999	99.999
4437777711669788416	244.96412	5.29721	39	33	35	0.46976	16.403	16.598	16.067	0.078	0.074
4113412916685330304	254.11532	−24.06865	36	30	28	0.47605	16.5	16.869	15.891	0.07	0.082
4311050922079027584	285.55926	10.57317	18	15	13	0.47706	18.337	19.361	17.269	0.158	99.999
3099348185775497728	101.98331	−7.41384	19	17	16	0.48199	14.245	14.649	13.646	99.999	99.999
4114405122877842688	257.82295	−23.27459	21	17	19	0.48384	16.982	17.432	16.387	0.186	0.425
5958267083020200448	263.74736	−44.83491	22	21	22	0.48582	15.313	15.668	14.777	0.126	99.999
1454878497455250048	205.5597	28.42065	45	44	42	0.48612	15.315	15.451	14.968	0.09	0.11

Continuation

ϕ_{21}	ϕ_{31}	ϖ	σ_{ϖ}	E(BR/RP)	ϵ_i	D	RUWE	Classification	New	Notes
rad	rad	mas	mas		mas					
(13)	(14)	(15)	(16)	(17)	(18)	(19)	(20)	(21)	(22)	(23)
99.999	99.999	0.855	0.03	1.205	0.0	0.0	0.965	OTHER	–	(a)
0.838	0.395	0.415	0.078	1.344	0.0	0.0	1.013	RRC	–	–
2.439	99.999	−0.096	0.089	1.217	0.091	0.355	1.044	RRC	–	(a)
3.251	99.999	0.068	0.077	1.301	0.0	0.0	0.999	RRAB	–	(a), (e)
1.688	2.749	0.123	0.076	1.279	0.0	0.0	1.032	OTHER	–	–
2.243	99.999	0.177	0.026	1.199	0.108	3.37	1.228	RRC	N	(f), (g)
2.012	99.999	0.018	0.084	1.245	0.167	1.133	1.079	OTHER	–	–
99.999	99.999	0.401	0.103	1.274	0.45	10.49	1.599	RRAB	–	(a)
2.393	5.797	0.046	0.066	1.208	0.0	0.0	0.985	OTHER	–	–
1.695	5.894	0.107	0.086	1.247	0.0	0.0	1.003	OTHER	–	–
2.451	99.999	0.064	0.207	1.447	0.55	1.565	1.051	–	–	NC:(c), (e)
99.999	99.999	0.229	0.032	1.237	0.0	0.0	0.911	RRAB	–	(a)
1.914	1.335	−0.127	0.128	1.311	0.0	0.0	1.023	RRAB	–	–
1.898	99.999	0.04	0.041	1.234	0.0	0.0	1.065	DCEP_1O	N	–
2.299	4.807	−0.045	0.035	1.234	0.0	0.0	0.993	RRC	–	(h)

Notes. The different columns correspond to the following: (1) *Gaia* DR2 source identification; (2)–(3) RA–Dec (J2000); (4)–(6) number of epochs in G, G_{BP}, and G_{RP}, respectively; (7) period; (8)–(10) intensity averaged magnitudes in G, G_{BP}, and G_{RP}, respectively; (11)–(12) and (13)–(14) Fourier amplitude ratios and Fourier phase differences; (15)–(16) parallax and parallax error; (17) excess of flux in the BP and RP integrated photometry with respect to the G band; (18)–(19) excess noise of the source and its significance; (20) renormalised unit weight error (see text); (21) new variability classification from present work; (22) flag "N" to denote a cepheid not known in the literature; (23) notes: (a) wrong period in DR2, used the literature or derived in this work; (b) uncertain period; (c) uncertain astrometry; (d) incomplete LC; (e) scattered LC; (f) bad astrometric solution (see text); (g) classification based on the LC shape; (h) adopted literature classification; (i) uncertain classification of LC shape. We note that when a numeric value is missing we assigned the value "99.999", whereas in case of empty string fields, we display a "–" string. The table is published in its entirety at the CDS. A portion including the first 15 lines is shown for guidance regarding its form and content.

hosted by a stellar systems such as Galactic open or globular clusters (OC; GC) or by dwarf galaxies orbiting the MW. To reach our goal, we first inspected the literature and then tested new possible associations. As for the literature, we relied on the work by Anderson et al. (2013) and by Clement et al. (2001) for the association between DCEPs and open clusters and between RRLs/ACEPs/T2CEPs, and GCs. Different sources were adopted for the association with dwarf galaxies in the local group. The result of this work is reported in Table 7. An inspection of the table shows that 53 and 66 Cepheids of different types were already known from the OGLE survey to be hosted by LMC and SMC, respectively.

We also searched additional associations between Cepheids in the MW sample and the above quoted stellar systems. However, we did not investigate new associations between DCEPs and OCs, as this complex work would deserve an entire new paper. We searched new MCs objects by simply overlapping the Cepheids in the surroundings of these galaxies (i.e. from $-56° \leq$ Dec $\leq -80°$, 0h $\leq$ Ra $\leq$ 4h and 4h $\leq$ Ra $\leq$ 8h for the SMC and LMC, respectively) with the precise PL/PW relations holding for these systems. In case an object with a certain cepheid type falls within 3σ of the relative PL/PW sequences (Table 1), we considered a positive match and assigned the object to the LMC or SMC. In this way we assigned 8 and 7

Table 6. Comparison of the reclassified object with the literature.

	DCEP_F	DCEP_1O	DCEP_2O	DCEP_M	ACEP_F	ACEP_1O	BLHER	WVIR	RVTAU	RRAB	RRC	OTHER	CEP	NC
DCEP_F	449	6	0	1	5	0	16	19	1	0	0	14	2	7
DCEP_1O	7	129	0	0	0	1	4	2	0	0	0	6	0	0
DCEP_2O	0	0	1	0	0	0	0	0	0	0	0	0	0	0
DCEP_M	0	0	0	16	0	0	0	0	0	0	0	1	0	1
ACEP_F	7	0	0	0	54	1	5	0	0	0	0	0	0	0
ACEP_1O	0	0	0	0	0	2	0	0	0	0	0	0	0	0
BLHER	10	5	0	0	3	1	56	0	0	0	0	3	4	0
WVIR	4	0	0	0	0	0	0	89	5	0	0	11	1	8
RVTAU	0	0	0	0	0	0	0	2	22	0	0	7	0	16
RRAB	1	0	0	0	18	0	8	0	0	79	0	0	0	5
RRC	0	1	0	0	0	0	0	0	0	0	2	0	0	1
OTHER	29	12	0	0	1	0	4	10	19	0	1	179	0	42
NEW	68	51	0	3	21	1	49	24	1	1	1	426	6	86
TOTAL	575	204	1	20	102	6	142	146	48	80	4	647	13	128

Notes. Columns and rows show the classification given in this work and in the literature, respectively. The "NEW" and "TOTAL" rows show the number of new objects found in this work and the total number for each pulsating class.

new Cepheids of different types to the LMC and SMC, respectively (see Table 7 for details). Thus we have a total of 61 and 73 Cepheids hosted by the LMC and SMC, respectively. These objects were then used to derive the PL/PW relations for the MCs calculated in Sect. 2 and listed in Table 1. The effect of the few tens DCEPs added to the LMC/SMC samples is insignificant, whereas the addition of the ACEPs increased the sample significantly.

As for the possible association with GCs or other dwarf galaxies in the local group, we cross-matched the position of the Cepheids in the MW sample with the positions of these objects, looking for objects within the tidal radii of GCs or within twice the semimajor axes of the dwarf galaxies; we adopted Harris (1996) or McConnachie (2012) for the positions and tidal radii or semimajor axes values for clusters or dwarf galaxies, respectively. We then used *Gaia* DR2 photometry and proper motions (PMs) to check if the target has a position in the colour-magnitude diagram (CMD) and PMs compatible with the rest of the stars of the investigated system. As a result of this exercise, we were able to associate 1 ACEP_F variable with the URSA MINOR dwarf spheroidal galaxy, 1 WVIR pulsator with the GC NGC 6254, and a variable of unknown type to NGC 6266 (see Table 7).

3.2.2. Distribution of the MW DCEPs on the Galactic plane

To further show the properties of the clean DCEPs sample, it is interesting to investigate the distribution of these pulsators on the Galactic plane. To this aim, we first calculate the Galactocentric Cartesian distances by subtracting the heliocentric space vector of the Galactic centre, $\boldsymbol{D}_0$ from the heliocentric space vector of our targets $\boldsymbol{D}_\odot$ as follows:

$$\boldsymbol{D}_{\rm GC} = \boldsymbol{D}_\odot - \boldsymbol{D}_0 \tag{3}$$

or

$$\begin{pmatrix} X \\ Y \\ Z \end{pmatrix} = \begin{pmatrix} d\cos(b)\cos(l) \\ d\cos(b)\sin(l) \\ d\sin(b) \end{pmatrix} - \begin{pmatrix} D_0 \\ 0 \\ 0 \end{pmatrix}, \tag{4}$$

where D_0 is the distance of the Sun from the Galactic centre and l, b, and d the Galactic longitude, Galactic latitude, and heliocentric distance, respectively, of each DCEP. The heliocentric distances d in kpc were obtained from the PW obtained for the MW DCEP_F sample (first line of Table 3, see next section) using the simple equation

$$d = 10^{0.2(W-W_{\rm A})-2}, \tag{5}$$

where W and $W_{\rm A}$ are the apparent and absolute Wesenheit magnitudes, respectively. We also used the same procedure for DCEP_1O (because their PW relation is much more uncertain), by fundamentalising their periods using the equation $P_{\rm F} = P_{\rm 1O}/(0.716 - 0.027\log P_{\rm 1O})$, where $P_{\rm F}$ and $P_{\rm 1O}$ are the periods of DCEP_F and DCEP_1O, respectively (Feast & Catchpole 1997). Finally, the distance of the targets from the Galactic centre is given as

$$R_{\rm GC} = \sqrt{[d\cos(b)\cos(l) - D_0]^2 + d^2\cos(b)^2\sin(l)^2 + d^2\sin(b)^2}. \tag{6}$$

The distribution of DCEPs on the Galactic plane is shown in the top panel of Fig. 6, where known and newly discovered DCEPs are depicted with blue and red symbols, respectively. The figure shows that, as expected, most of the known pulsators are placed within few kiloparsec from the Sun, whereas the majority of the new sources are further away. We also note that the DCEPs investigated in this work trace the Local Arm and the Perseus Arm. It is also interesting to look at the distribution of the pulsators around the Galactic plane. This is shown in the bottom panel of Fig. 6, where we plot the height (Z) of each object as a function of the Galactocentric distance $R_{\rm GC}$ for selected intervals of the Galactocentric angular coordinate Φ that is 0 in the direction of the Sun and increases counterclockwise. The figure clearly shows the presence of the well-known disc warp, especially for $0° < \Phi < 120°$. These results are in agreement with the works by Chen et al. (2019) and Skowron et al. (2018), who used different DCEP samples to study the warp of the MW disc. A detailed discussion of the warp as traced by DCEPs is beyond the scope of present paper and the works cited provide in-depth discussions on the arguments.

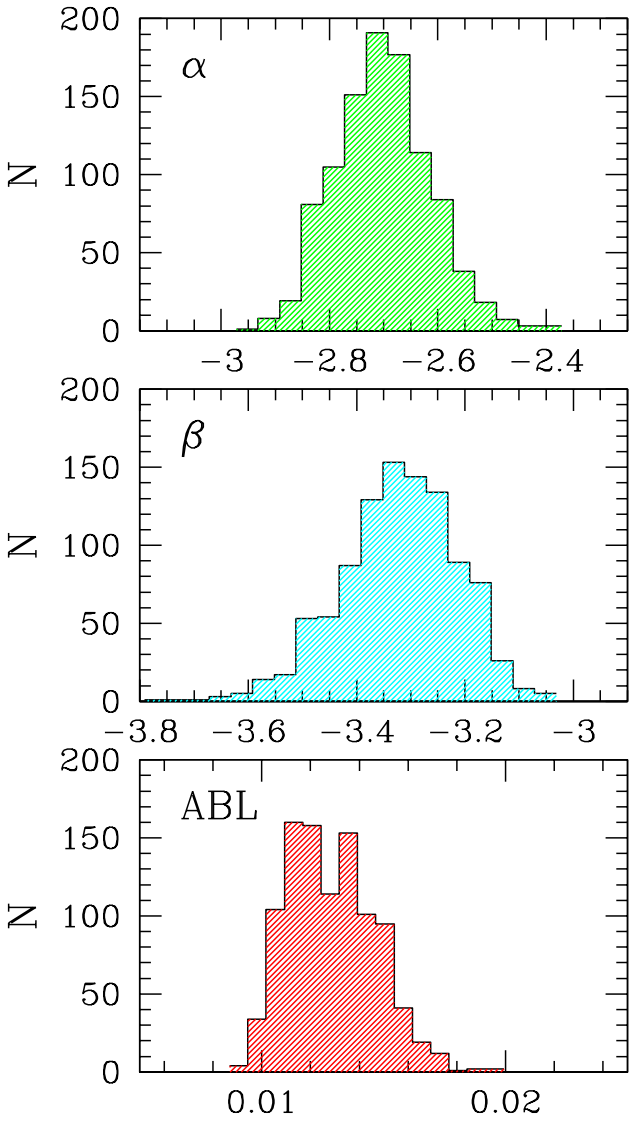

Fig. 7. Example of the results of the bootstrap procedure described in the text in the case of the PW in the form $W_A = \alpha + \beta \log P$ applied to DCEP_F. *From top to bottom*, the different panels show the distribution of the parameters α, β and of the residuals of data around the ABL function, respectively.

4. PW relations for MW Cepheids

The new dataset of reclassified Cepheids allows us to derive the PW relation directly from the data for MW DCEPs and T2CEPs. We preferred not to try with ACEPs because of the paucity of the sample and the considerable dispersion in the PW plane, resulting from the large parallax errors; ACEPs are generally significantly fainter than DCEPs. We note that the 107 DCEPs belonging to LMC/SMC (see Sect. 7) were excluded from the MW DCEP sample adopted for the following analysis to avoid contamination by much less metallic objects with respect to the MW sources. We decided not to exclude T2CEPs from both MCs and other GC/dwarf galaxies satellites of the MW because the properties of these objects are expected to be more homogeneous in different environments.

To use all the Cepheids in our sample we are forced to adopt only the Wesenheit magnitude, as we do not know individual reddenings for each cepheid, making impossible for the moment to derive meaningful PL relations. Similarly, we did not attempt to add a metallicity term in Eq. (7) (see below), as this information is lacking for a consistent part of our sample.

To derive the PW relations we decided to use the ABL defined below. We underline that the adoption of this quantity has the decisive advantage to use the parallax in a linear fashion, avoiding almost any kind of bias, as no selection is done on the cepheid sample. Indeed, the employment of the ABL allows us to include in the analysis objects with negative parallaxes. A detailed discussion of the advantages of the ABL method is provided in other papers (see e.g. Arenou & Luri 1999; Gaia Collaboration 2017).

The ABL for the absolute Wesenheit magnitude W_A is defined as follows:

$$\mathrm{ABL} = 10^{0.2W_A} = 10^{0.2(\alpha+\beta\log P)} = \varpi 10^{0.2W-2}, \quad (7)$$

where we used the definition of PW relation: $W_A = \alpha + \beta \log P$; W_A and W are the absolute and relative Wesenheit magnitudes, respectively. The observed quantities are W, P, and ϖ. The unknown α and β values can be obtained using a least-squares fit procedure.

We applied this technique to estimate the PW relations for DCEP_F, DCEP_1O, and T2CEP, where this last sample includes only BLHER and WVIR as above for the LMC and SMC. In more detail, the fitting procedure has been carried out using the nonlinear least-squares (*nls*) routine included in the *R* package[7]. We adopted a weighted fitting conjugated with the bootstrap method to measure robust errors on the parameters of the fit. In practice, the procedure is repeated 1000 times and for each bootstrap we obtained a value of α and β; we increased the number of bootstraps until the results did not depend on this number. The average values for these parameters and their standard deviations are obtained from the resulting distributions. An example of the results is shown in Fig. 7, where the distributions of α and β are reported, as well as that of the residuals around the ABL function. The results of the fitting procedure for the different cases are shown in the first three rows of Table 3.

A comparison of the PW slopes between LMC and MW in Tables 1 and 3 reveals that the slopes of the PW relations for the DCEP_F and T2CEPs are completely consistent with each other within the errors, whereas for DCEP_1O the discrepancy is of the order of 2σ level, where the slope of the MW sample is steeper than that of LMC. However the large error on the slope of the MW sample makes this comparison not very stringent.

We note that the low dependence on metallicity of the slope for DCEP_Fs is in agreement with previous works (both in theoretical and observational) as it is generally found that the slope of the PW for many different band combinations has a very small dependence on the metallicity (see e.g. Fiorentino et al. 2007, 2013; Ngeow et al. 2012; Di Criscienzo et al. 2013; Gieren et al. 2018, and references therein). We return to this argument in the next section. Similarly, for T2CEPs we do not find a significant dependence of the slope of the PW on the average metallicity of the parent population, again in agreement with literature (see e.g. Matsunaga et al. 2009, 2011; Ripepi et al. 2015).

To the aim of comparing the zero points of the PW relations holding for MW and LMC, we imposed the proper values of β for the LMC in Eq. (7) and rerun the fitting procedure with the same modality as before. The result of this operation is reported in the second series of three rows in Table 1 and graphically in the right panels of Fig. 3. As expected the zero points of the relations for DCEP_Fs and T2CEPs are not significantly

[7] http://www.R-project.org/

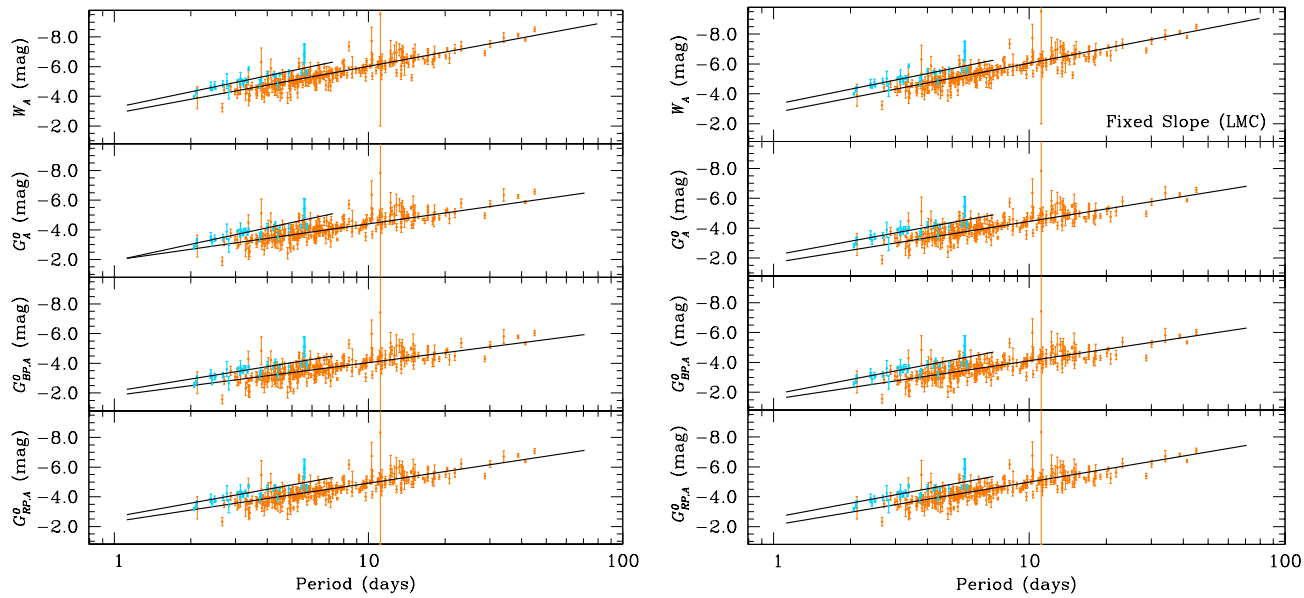

Fig. 8. Resulting PL/PW relations for the MW selected sample of DCEPs having reddening estimate and intensity averaged magnitudes in G, G_{BP} and G_{RP} bands coming from the *Cepheids&RRLyrae* SOS pipeline. Orange and light blue symbols represent DCEP_F and DCEP_1O, respectively. The solid lines are the least-squares fits to the data obtained using the ABL formulation (see text). As in Fig. 3, *left* and *right panels* show the relations obtained leaving all the parameters free to vary and fixing the value of β in Eq. (7), respectively. The coefficient of the regression lines are shown in Table 3. An underscript "A" means absolute magnitudes whereas a superscript 0 characterises de-reddened quantities.

Table 7. Association of pulsator in the all sky sample with open/globular clusters and with dwarf galaxies satellites of the MW.

Source_id (1)	Lit. name (2)	Classification (3)	Host system (4)	Source of association (5)
428620663657823232	DL Cas	DCEP_F	NGC129	A13
429385923752386944	CG Cas	DCEP_F	Berkeley58	A13
2011892320749270912	CE Cas B	DCEP_F	NGC7790	A13
2011892325047232256	CE Cas A	DCEP_F	NGC7790	A13
2011892703004353792	CF Cas	DCEP_F	NGC7790	A13
2031776202613700480	SU Cyg	DCEP_F	Turner9	A13
4085919765884068736	BB Sgr	DCEP_F	Collinder394	A13
4092905375639902464	U Sgr	DCEP_F	IC4725	A13
4094784475310672128	WZ Sgr	DCEP_F	Turner2	A13
4156512638614879104	EV Sct	DCEP_1O	NGC6664	A13
5835124087174043136	S Nor	DCEP_F	NGC6087	A13
5891675303053080704	V Cen	DCEP_F	NGC5662	A13
5932565900081831040	QZ Nor	DCEP_1O	NGC6067	A13
5932569709575669504	V340 Nor	DCEP_F	NGC6067	A13
2957940098405233024	V7	WVIR	NGC1904	C01

Notes. The different columns correspond to the following: (1) *Gaia* DR2 source identification; (2) name of the object in the literature (if any); (3) type of variability according to this work; (4) host system; (5) source of the association of the variable with the stellar system. The table is published in its entirety only at the CDS. A portion including the first 15 lines is shown for guidance regarding its form and content.
References. A13 (Anderson et al. 2013); B05 (Bersier & Wood 2002); C01 (Clement et al. 2001); CO15 (Coppola et al. 2015); DR1 (Clementini et al. 2016); EROS2_KIM (Kim et al. 2014); K08 (Kinemuchi et al. 2008); MV16 (Martínez-Vázquez et al. 2016); OGLE (Optical Gravitational Lensing Experiment, Soszyński et al. 2015a,b, 2016, 2017a,b, 2018); TW (This work).

different than in the previous case, whereas the contrary is true for DCEP_1Os. We use these results in Sect. 4.2.

As a final note, we underline that because of the lack of thorough information in the literature, in this work we do not consider the source of uncertainty represented by the duplicity among DCEPs whose incidence is highly uncertain, but estimated to be as large as 35–50% or even more (see Anderson & Riess 2018, and references therein). The presence of companions for DCEPs affects not only the parallaxes measured by *Gaia* (duplicity is not taken into account in DR2), but also their photometry, thus possibly representing a potential significant source of uncertainty. The future *Gaia* data releases will allow us to also face this important issue.

4.1. PL relations in G, G_{BP}, and G_{RP} bands for MW DCEPs

To the aim of providing PL relations in the *Gaia* G, G_{BP}, and G_{RP} bands for the MW Cepheids, we need an estimate of the reddening. As the *Gaia* DR2 does not include reliable interstellar extinctions yet, we have to use literature data. Thus, we found

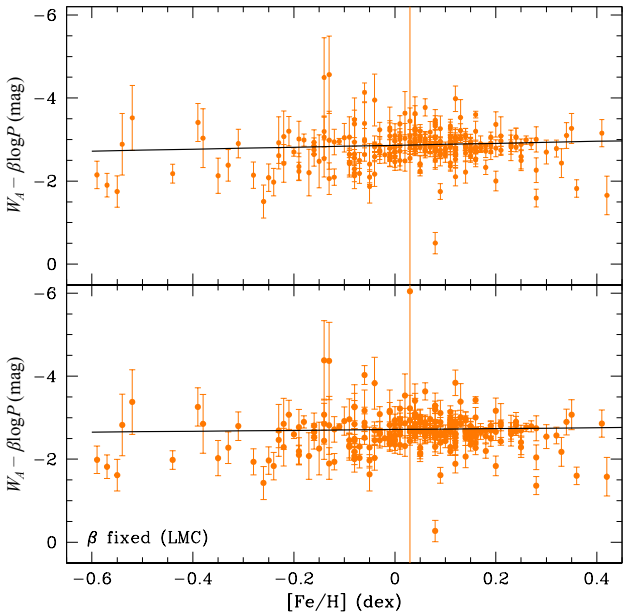

Fig. 9. Dependence of the PW relation from [Fe/H]. Orange symbols represent DCEP_F pulsators, whereas the solid lines are the results of the fitting procedure for the ABL formulation of Eq. (11) in two cases: (i) all parameters free to vary (*top panel*); (ii) β parameter fixed to the value of LMC (*bottom panel*). The coefficient of the regression lines are shown in the last two lines of Table 3.

that reliable $E(B-V)$ values are available for a subsample of 301 objects classified as DCEPs in Table 5. The main source for the reddening was Fernie (1990), whereas additional values were taken from Majaess et al. (2008), Ngeow (2012), and Kashuba et al. (2016). Only a few objects possess reliable reddening estimates among MW T2CEPs, therefore we did not try to calculate PLs for these objects. As for the metallicity, we used the results by Genovali et al. (2013, 2014, 2015).

The reddening values found in the literature are listed in Table 8 together with the mode of pulsation (268 and 33 DCEP_Fs and DCEP_1Os, respectively), metallicity estimate, and sources for reddening and metallicity, respectively (last two columns).

Before proceeding, we first have to estimate the absorption in the *Gaia* bands in terms of $E(B-V)$. To this aim we used again the Jordi et al. (2010) tables, and adopting the same procedure outlined in Sect. 2, we obtained starting values of 2.90, 3.60, and 2.15 for the ratios $A(G)/E(B-V)$, $A(G_{BP})/E(B-V)$, and $A(G_{RP})/E(B-V)$, respectively.

We used again the ABL formulation of Eq. (7) and the bootstrap technique to derive the relevant PL/PW relations. Now the observed magnitudes in the exponent of the right term can be the apparent Wesenheit W or the observed de-reddened magnitudes G^0, G^0_{BP}, and G^0_{RP}. With this formulation and the same procedure of Sect. 4 we calculated the PL relations in the *Gaia* G, G_{BP}, and G_{RP} band for the MW DCEPs subsample described above. Analysing the dispersion of the residuals, we checked the above defined total-to-selective extinction ratios, by varying their values and re-estimating the dispersion of the residuals (of the ABL) at any step. We retained the ratio values that returned the smallest dispersions. These values are shown in Eqs. (8)–(10), where the uncertainties were estimated by looking at the values of total-to-selective extinction ratios that produced an increase in the dispersion. We remark that, owing to the large G, G_{BP} and G_{RP} bandwidths, these total-to-selective ratios are only valid in the interval of colours spanned by Cepheids. These relations are written as

$$A(G) = (2.70 \pm 0.05)E(B-V), \quad (8)$$

$$A(G_{BP}) = (3.50 \pm 0.10)E(B-V), \quad (9)$$

$$A(G_{RP}) = (2.15 \pm 0.05)E(B-V). \quad (10)$$

Finally, adopting the relations of Eqs. (8)–(10) we calculated the PL relations in the *Gaia* G, G_{BP}, and G_{RP} band for the MW DCEPs subsample. The results are shown in the second part of Table 3 and Fig. 8. We note that we also recalculated the PW using the subsample adopted here. An inspection of Table 3 shows agreement within 1σ between the PWs derived using the full sample and subsample of DCEP_Fs. The same comparison is less meaningful for DCEP_1Os because of the huge errors caused by the intrinsic large dispersion of the full sample and by the small statistic in the case of the subsample.

As for the subsample discussed in this section we also have the information about metallicity available (see Table 8); we tried to derive PW relations using the following ABL definition including an additional term to take into account the dependence of the zero point on the metallicity [Fe/H] as follows:

$$\mathrm{ABL} = 10^{0.2W_A} = 10^{0.2(\alpha+\beta\log P+\gamma[\mathrm{Fe/H}])} = \varpi 10^{0.2W-2}, \quad (11)$$

where W_A and W are the absolute and relative Wesenheit magnitudes, respectively. In principle, the β term also depends on metallicity, but a comparison of the slopes for DCEP_Fs in the LMC (Table 1) and MW (first line of Table 3), shows that the dependence of β on metallicity can be expected reasonably low to be ignored. As this is not true for the PLs, in the following we use only the Wesenheit magnitudes.

Adopting the usual bootstrap technique applied to the ABL formulation of Eq. (11), we obtain the result reported in the penultimate line of Table 3 and Fig. 9. The derived metallicity term $\gamma = -0.237 \pm 0.199$ dex mag^{-1}, even if only barely significant (1σ), means that at fixed period and colour, metal poor stars are fainter. These results are in good agreement with Groenewegen (2018) who derived PL/PW relations in the optical and near-infrared bands adopting a subsample of DCEPs with *Gaia* DR2 parallaxes and literature photometry/spectroscopy and also with theoretical predictions for the dependence of DCEP optical PW functions on metallicity (see Fig. 9 in Caputo et al. 2000). Again, to compare the results for the MW and LMC, we recalculated the ABL of Eq. (11) but imposed the LMC value for the term β. The outcome of this exercise is shown in the last line of Table 3 and Fig. 9. Not surprisingly, the metallicity term becomes much less significant, as part of the metallicity dependence has been absorbed by the variation of the slope.

To obtain more stringent constraint on the dependence of DCEP PW and PL relations on metallicity we require the more precise parallaxes expected in the next *Gaia* releases; we also need to increase the sample of DCEPs possessing accurate and homogeneous measurements of metallicity by means of high resolution spectroscopy, possibly extending the metallicity range spanned by the MW DCEPs analysed in this work. In fact, only a few objects reach a metallicity value as low as that of the LMC ([Fe/H] ~ -0.4 dex); the large majority of the pulsators cluster around [Fe/H] $\sim +0.05 \pm 0.13$ dex (see Table 8).

4.2. Distance of the LMC and zero points of the Gaia DR2 parallaxes for Cepheids

In the previous sections we estimated the PW relations in the *Gaia* bands for both the LMC and the MW using the slopes of the LMC. This operation makes it straightforward to estimate the distance of the LMC, that is an important anchor for the extragalactic distance scale, by comparing the zero points

Table 8. Reddening and metallicity for the 301 known MW Cepheids having *Gaia* DR2 intensity averaged magnitudes in the G, G_{BP}, and G_{RP} bands coming from the *Cepheids&RRLyrae* SOS pipeline.

Name	Mode	Source_id	$E(B-V)$ mag	$\sigma E(B-V)$ mag	[Fe/H] dex	Ref1	Ref2
(1)	(2)	(3)	(4)	(5)	(6)	(7)	(8)
AA Gem	DCEP_F	3430067092837622272	0.380	0.019	−0.14	1	5
AC Cam	DCEP_F	462252662762965120	0.915	0.046	−0.16	1	5
AC Mon	DCEP_F	3050050207554658048	0.539	0.035	−0.06	1	5
AD Cam	DCEP_F	462407693902385792	0.929	0.013	−0.28	1	5
AD Cru	DCEP_F	6057514092119497472	0.681	0.013	0.08	1	5
AD Gem	DCEP_F	3378049163365268608	0.173	0.019	−0.14	1	5
AD Pup	DCEP_F	5614312705966204288	0.386	0.021	−0.06	1	5
AE Vel	DCEP_F	5309174967720762496	0.735	0.058	0.11	1	5
AG Cru	DCEP_F	6059635702888301952	0.257	0.021	0.05	1	5
AH Vel	DCEP_1O	5519380077440172672	0.038	0.020	0.09	1	5

Notes. The different columns correspond to the following: (1) literature name; (2) mode of pulsation; (3) *Gaia* DR2 source identification; (4)–(5) $E(B-V)$ and error on its value; (6) metallicity ([Fe/H] value); (7)–(8) reference for $E(B-V)$ and [Fe/H], respectively. We note that the errors on metallicity are not provided as these are usually not available object by object. They can be estimated to be ∼0.1–0.15 dex. The table is published in its entirety at the CDS. A portion including the first 10 lines is shown for guidance regarding its form and content.
References. 1 = Fernie (1990); 2 = Ngeow (2012); 3 = Majaess et al. (2008); 4 = Kashuba et al. (2016); 5 = Genovali et al. (2013, 2014, 2015).

Table 9. Results for the distance of LMC (see text).

Type	DM (mag)	[Fe/H] term
DCEP_F	18.699 ± 0.024	No
DCEP_F	18.673 ± 0.085	Yes
T2CEP	18.587 ± 0.065	No

of the relative and absolute PWs in the LMC and MW, respectively. We performed this exercise for DCEP_Fs and T2CEPs as the PW for DCEP_1Os is too uncertain. For DCEP_Fs we used both the PW without and with the metallicity term. In this last case we adopted [Fe/H] = −0.43 dex for the LMC (Mucciarelli et al. 2011), whereas for the MW we took the average of the distribution of metallicities listed in Table 8, i.e. [Fe/H] = +0.05 ± 0.13 dex. The results are reported in the second column of Table 9, where the errors on the distance moduli (DMs) have been calculated summing in quadrature the uncertainties on the zero points (α terms) and the metallicity (γ) when needed (see Tables 1 and 3). As a result, the DM_{LMC} obtained are always significantly longer than the commonly accepted value of ∼18.50 mag (see e.g. Pietrzyński et al. 2013; de Grijs et al. 2014; Riess et al. 2018b), even if the parallax zero point correction of +0.046 mas by Riess et al. (2018b) has already been applied.

Conversely, if we use this value for the LMC distance as reference, we can recalculate the zero point offset of the *Gaia* DR2 parallaxes, discovering that the parallaxes zero point offset needed to obtain a $DM_{LMC} \sim 18.50$ mag is of the order of +0.1 and +0.07 mas for the DCEP_F and T2CEPs, respectively. These results are agree well with a similar analysis carried out by Groenewegen (2018), which provides a more detailed discussion.

5. Summary

In this paper we have re-analysed the sample of Cepheids published in the context of *Gaia* DR2 by Clementini et al. (2019). The main achievements of this work are the following:

– We calculated the PL/PW relations in the *Gaia* bands G, G_{BP} and G_{RP} for all the cepheid types (DCEP, ACEP, T2CEP) both in the LMC and SMC. These relations will be incorporated in the next versions of the *Gaia Cepheids&RRLyrae* SOS pipeline adopted to classify the Cepheids in the *Gaia* DR3 (see Clementini et al. 2019).
– We carried out a careful re-analysis of the classification of the 2116 Cepheids of all types reported by Clementini et al. (2019) as belonging to the MW. We first conducted a literature search for alternative classification and period determination for these objects. Afterwards we reclassified each object by visually inspecting its LC and position in the PW and period-Fourier parameters.
As a result, a total of 1257 stars were classified as cepheid of any type, 84 objects as RR Lyrae, and 647 as variables of other type (in addition to the 128 stars with no classification). Among these 1257 Cepheids, 713 were Cepheids already known in the literature, 274 are new Cepheids completely unknown in the literature or indicated generically as variable, and 270 objects were known in the literature with a different classification. In total we classified 800 DCEPs, 108 ACEPs, and 336 T2CEPs, plus 13 Cepheids for which we were not able to find an appropriate subclassification in type.
Among the MW sample we individuated a total of 61 and 73 Cepheids of different types hosted by the LMC and SMC, of which 8 and 7 of these samples were not known in the literature as LMC/SMC objects.
In addition, we were able to associate an ACEP_F variable with the URSA MINOR dwarf spheroidal galaxy, a WVIR pulsator with the GC NGC 6254, and a variable of unknown type to NGC 6266.
– Using the reclassified cepheid sample, we used the ABL formulation to derive PW relations in the *Gaia* bands for the MW DCEP_F, DCEP_1O and T2CEP (BLHER and WVIR). The use of the ABL formulation allows us to derive slopes and zero points for the PW that are almost unbiased, as we did not carry out any kind of selection on the sample. The adoption of a subsample (301 objects) of well-characterised MW DCEPs possessing reliable reddening and metallicity estimates, also allowed us to calculate the PL relations for the G, G_{BP}, and G_{RP} bands for DCEP_F and DCEP_1O.
In addition, using the quoted subsample, we were able to investigate for the first time the dependence on metallicity of the PW relation for DCEP_Fs in the *Gaia* bands. As a result, we derived a modestly significant (1σ) dependence ($\gamma = -0.237 \pm 0.199$ dex mag^{-1}), in the sense that at fixed

period and colour metal poor stars are fainter. More precise parallaxes and spectroscopic measures will be needed to address firmly this point.
– We also calculated the PW relations for the MW by imposing the slope of the PW relations in the LMC and redetermining the zero points. By comparing the relative zero points between the MW and the LMC PW for DCEP_F and T2CEP, we obtained two different estimates of the LMC distance. These values are larger than the usually accepted value for the LMC DM ∼ 18.50 mag. To reconcile the results found in this work with the latter, we need to increase the zero points of the *Gaia* DR2 parallax by at least 0.07 mas, in agreement with recent literature results.

The *Gaia* DR2 photometry and parallax for Cepheids in the MW allowed a significant step forward in the classification of the different type of Cepheids. Indeed, the excellent photometric quality, even conjugated the relatively low-accurate parallaxes for the sample of objects discussed in this paper, allowed us to revise the literature classification for more than 200 objects.

In conclusion, without entering in details beyond the scope of present paper, the results presented in this work seem to confirm the Groenewegen (2018) suggestion that the parallaxes for MW Cepheids in the *Gaia* DR2, appear still too uncertain to allow a significative decrease of the error on the value of H_0. To this we have to add the uncertainties on the extinction law, the impact of metallicity, and binarity, affecting both astrometry and photometry of Cepheids.

Great improvements are awaited from the future *Gaia* DR3 and DR4 for all these issues. Indeed, these releases are expected to present extremely accurate photometry and astrometry corrected for the effect of multiplicity, as well as individual information on reddening, metallicity, and duplicity for a large portion of the sky. Therefore, DR3 and DR4 will certainly allow us to make consistent steps forward in the accuracy of the extragalactic distance scale, helping to reduce the uncertainty on the value of H_0 to less than 1%.

Acknowledgements. We thanks our anonymous referee whose comments helped to improve the paper. We gratefully thank G. Clementini for stimulating discussions on the subject of this paper. This work has made use of data from the European Space Agency (ESA) mission *Gaia* (https://www.cosmos.esa.int/gaia), processed by the *Gaia* Data Processing and Analysis Consortium (DPAC, https://www.cosmos.esa.int/web/gaia/dpac/consortium). Funding for the DPAC has been provided by national institutions, in particular the institutions participating in the *Gaia* Multilateral Agreement. In particular, the Italian participation in DPAC has been supported by Istituto Nazionale di Astrofisica (INAF) and the Agenzia Spaziale Italiana (ASI) through grants I/037/08/0, I/058/10/0, 2014-025-R.0, and 2014-025-R.1.2015 to INAF (PI M.G. Lattanzi). This research has made use of the International Variable Star Index (VSX) database, operated at AAVSO, Cambridge, Massachusetts, USA. This research has made use of the SIMBAD database, operated at CDS, Strasbourg, France

References

Alfonso-Garzón, J., Domingo, A., Mas-Hesse, J. M., & Giménez, A. 2012, A&A, 548, A79
Anderson, R. I., & Riess, A. G. 2018, ApJ, 861, 36
Anderson, R. I., Eyer, L., & Mowlavi, N. 2013, MNRAS, 434, 2238
Andrae, R., Fouesneau, M., Creevey, O., et al. 2018, A&A, 616, A8
Arenou, F., & Luri, X. 1999, Harmonizing Cosmic Distance Scales in a Post-Hipparcos Era, 167, 13
Berdnikov, L. N., Kniazev, A. Y., Sefako, R., et al. 2015, Astron. Lett., 41, 23
Bersier, D., & Wood, P. R. 2002, AJ, 123, 840
Caputo, F., Marconi, M., & Musella, I. 2000, A&A, 354, 610
Catelan, M., & Smith, H. A. 2015, Pulsating Stars (Wiley-VCH)
Chen, X., Wang, S., & Deng, L. 2019, Nat. Astron., 202, 33
Clement, C. M., Muzzin, A., Dufton, Q., et al. 2001, AJ, 122, 2587
Clementini, G., Ripepi, V., Leccia, S., et al. 2016, A&A, 595, A133
Clementini, G., Ripepi, V., Molinaro, R., et al. 2019, A&A, 622, A60
Coppola, G., Marconi, M., Stetson, P. B., et al. 2015, ApJ, 814, 71
de Grijs, R., Wicker, J. E., & Bono, G. 2014, AJ, 147, 122
Di Criscienzo, M., Marconi, M., Musella, I., Cignoni, M., & Ripepi, V. 2013, MNRAS, 428, 212
Drake, A. J., Graham, M. J., Djorgovski, S. G., et al. 2014, ApJS, 213, 9
Drake, A. J., Djorgovski, S. G., Catelan, M., et al. 2017, MNRAS, 469, 3688
Debosscher, J., Blomme, J., Aerts, C., & De Ridder, J. 2011, A&A, 529, A89
Dubath, P., Rimoldini, L., Süveges, M., et al. 2011, MNRAS, 414, 2602
Feast, M. W., & Catchpole, R. M. 1997, MNRAS, 286, L1
Fernie, J. D. 1990, ApJS, 72, 153
Fiorentino, G., Marconi, M., Musella, I., & Caputo, F. 2007, A&A, 476, 863
Fiorentino, G., Musella, I., & Marconi, M. 2013, MNRAS, 434, 2866
Gaia Collaboration (Prusti, T., et al.) 2016, A&A, 595, A1
Gaia Collaboration (Clementini, G., et al.) 2017, A&A, 605, A79
Gaia Collaboration (Brown, A. G. A, et al.) 2018, A&A, 616, A1
Genovali, K., Lemasle, B., Bono, G., et al. 2013, A&A, 554, A132
Genovali, K., Lemasle, B., Bono, G., et al. 2014, A&A, 566, A37
Genovali, K., Lemasle, B., da Silva, R., et al. 2015, A&A, 580, A17
Gieren, W., Storm, J., Konorski, P., et al. 2018, A&A, 620, A99
Groenewegen, M. A. T. 2018, A&A, 619, A8
Harris, W. E. 1996, AJ, 112, 1487
Hoffman, D. I., Harrison, T. E., & McNamara, B. J. 2009, AJ, 138, 466
Holl, B., Audard, M., Nienartowicz, K., et al. 2018, A&A, 618, A30
Ivezić, Ž., Smith, J. A., Miknaitis, G., et al. 2007, AJ, 134, 973
Jayasinghe, T., Kochanek, C. S., Stanek, K. Z., et al. 2018, MNRAS, 477, 3145
Jordi, C., Gebran, M., Carrasco, J. M., et al. 2010, A&A, 523, A48
Kashuba, S. V., Andrievsky, S. M., Chekhonadskikh, F. A., et al. 2016, MNRAS, 461, 839
Kim, D.-W., Protopapas, P., Bailer-Jones, C. A. L., et al. 2014, A&A, 566, A43
Kinemuchi, K., Harris, H. C., Smith, H. A., et al. 2008, AJ, 136, 1921
Leavitt, H. S., & Pickering, E. C. 1912, Harvard College Observatory Circular, 173, 1
Lemasle, B., Hajdu, G., Kovtyukh, V., et al. 2018, A&A, 618, A160
Lenz, P., & Breger, M. 2005, Commun. Asteroseismol., 146, 53
Lindegren, L. 2018, "Re-normalising the astrometric chi-square in *Gaia* DR2", Gaia Technical Note: GAIA-C3-TN-LU-LL-124-01
Lindegren, L., Hernández, J., Bombrun, A., et al. 2018, A&A, 616, A2
Madore, B. F. 1982, ApJ, 253, 575
Majaess, D. J., Turner, D. G., & Lane, D. J. 2008, MNRAS, 390, 1539
Martínez-Vázquez, C. E., Stetson, P. B., Monelli, M., et al. 2016, MNRAS, 462, 4349
Matsunaga, N., Feast, M. W., & Menzies, J. W. 2009, MNRAS, 397, 933
Matsunaga, N., Feast, M. W., & Soszyński, I. 2011, MNRAS, 413, 223
McConnachie, A. W. 2012, AJ, 144, 4
Mucciarelli, A., Cristallo, S., Brocato, E., et al. 2011, MNRAS, 413, 837
Ngeow, C.-C. 2012, ApJ, 747, 50
Ngeow, C.-C., Kanbur, S. M., Bellinger, E. P., et al. 2012, Ap&SS, 341, 105
Palaversa, L., Ivezić, Ž., Eyer, L., et al. 2013, AJ, 146, 101
Pietrzyński, G., Graczyk, D., Gieren, W., et al. 2013, Nature, 495, 76
Planck Collaboration Int. XLVI. 2016, A&A, 596, A107
Pojmanski, G. 1997, Acta Astron., 47, 467
Pojmanski, G. 2002, Acta Astron., 52, 397
Richards, J. W., Starr, D. L., Miller, A. A., et al. 2012, ApJS, 203, 32
Ripepi, V., Moretti, M. I., Marconi, M., et al. 2012, MNRAS, 424, 1807
Ripepi, V., Moretti, M. I., Marconi, M., et al. 2015, MNRAS, 446, 3034
Ripepi, V., Marconi, M., Moretti, M. I., et al. 2016, ApJS, 224, 21
Ripepi, V., Cioni, M.-R. L., Moretti, M. I., et al. 2017, MNRAS, 472, 808
Riess, A. G., Macri, L. M., Hoffmann, S. L., et al. 2016, ApJ, 826, 56
Riess, A. G., Casertano, S., Yuan, W., et al. 2018a, ApJ, 855, 136
Riess, A. G., Casertano, S., Yuan, W., et al. 2018b, ApJ, 861, 126
Samus', N. N., Kazarovets, E. V., Durlevich, O. V., Kireeva, N. N., & Pastukhova, E. N. 2017, Astron. Rep., 61, 80
Schönrich, R., McMillan, P., & Eyer, L. 2019, ArXiv e-prints [arXiv:1902.02355]
Sesar, B., Hernitschek, N., Mitrović, S., et al. 2017, AJ, 153, 204
Skowron, D. M., Skowron, J., Mróz, P., et al. 2018, ArXiv e-prints [arXiv:1806.10653]
Soszyński, I., Udalski, A., Szymański, M. K., et al. 2008, Acta Astron., 58, 293
Soszyński, I., Udalski, A., Szymański, M. K., et al. 2015a, Acta Astron., 65, 233
Soszyński, I., Udalski, A., Szymański, M. K., et al. 2015b, Acta Astron., 65, 329
Soszyński, I., Udalski, A., Szymański, M. K., et al. 2016, Acta Astron., 66, 131
Soszyński, I., Udalski, A., Szymański, M. K., et al. 2017a, Acta Astron., 67, 103
Soszyński, I., Udalski, A., Szymański, M. K., et al. 2017b, Acta Astron., 67, 297
Soszyński, I., Udalski, A., Szymański, M. K., et al. 2018, Acta Astron., 68, 89
Subramanian, S., & Subramaniam, A. 2015, A&A, 573, A135
Watson, C. L., Henden, A. A., & Price, A. 2006, Soc. Astron. Sci. Annu. Symp., 25, 47
Wenger, M., Ochsenbein, F., Egret, D., et al. 2000, A&AS, 143, 9
Woźniak, P. R., Vestrand, W. T., Akerlof, C. W., et al. 2004, AJ, 127, 2436

Appendix A: Acronyms for the literature variability types

In Table A.1 we expand the variability types adopted for Table 2.

Table A.1. Acronyms adopted in Table 2 to indicate the different variability types.

Acronym	Definition
ACEP_F	Anomalous Cepheids fundamental mode
ACEP_1O	Anomalous Cepheids first overtone
AGB	AGB star
AGN	Active galactic nuclei
BLHER	Type II cepheid BL Herculis
BLLac	BL Lacertae-type object
Be	Be eruptive stars
Carbon	Carbon star
CV	Cataclysmic variable
DCEP	Delta cepheid
DCEP_1O	Delta cepheid first overtone
DCEP_2O	Delta cepheid second overtone
DCEP_F	Delta cepheid fundamental mode
EB	Beta Lyrae-type eclipsing systems.
EB	Eclipsing binary
EC	Contact binaries
ELL	Rotating ellipsoidal variables
Em	Emission line star
Eruptive	Eruptive
ErupIRR	Eruptive irregular
FUOri	Fu Orionis type star
HB	Horizontal branch star
HS	Hot subdwarf star
Irr	Irregular
LPV	Long period variable
Mira	Variable star of Mira Cet type
NC	Not classified
Orion	Variable star of Orion type
PostAGB	Post AGB star
Puls	Pulsating variable star.
RC	Rapid change
RG	Red giant
ROT	Rotational
RR	RR Lyrae
RRab	RR Lyrae type ab
RRc	RR Lyrae type c
RSCVn	RS Canum Venaticorum type
RVTAU	RV Tauri type
SARG	Small amplitude red giant
SARG_A	Small amplitude red giant, subclass A
SARG_B	Small amplitude red giant, subclass AB
Semireg	Semiregular
SXPHE	Sx Phoenicis star
T2CEP	Type II cepheid
TTAU/CTTS	T Tauri star/classical T Tauri stars
UXOri	UX Orionis type star
VAR	Variable
WR	Wolf Rayet
WUma	W Uma
WVIR	Type II cepheid W Virginis
XRB	X-ray binary
YSO	Young stellar object